Title:

Endosomal-lysosomal organellar assembly (ELYSA) structures coordinate lysosomal degradation systems through mammalian oocyte-to-embryo transition

Authors:

Yuhkoh Satouh*[1], Takaki Tatebe[1], Isei Tanida[2], Junji Yamaguchi[2], Yasuo Uchiyama[2], Ken Sato*[1]

Affiliations:

1: Laboratory of Molecular Traffic, Institute for Molecular and Cellular Regulation, Gunma University, Maebashi, Japan.

2: Department of Cellular and Molecular Neuropathology, Juntendo University Graduate School of Medicine, Tokyo, Japan.

***Correspondence to:**

yuhkohs@gunma-u.ac.jp

sato-ken@gunma-u.ac.jp

Abstract:

Mouse oocytes mature from the germinal vesicle (GV) to meiosis II (MII) stage and are fertilized by a single sperm. After fertilization, the embryo degrades parts of the maternal components via lysosomal degradation systems, including autophagy and endocytosis, as zygotic gene expression begins during embryogenesis. Here, we demonstrate that endosomal-lysosomal organelles form assembly structures (ELYSAs) in the periphery of the oocyte plasma membrane. Small ELYSA structures appeared in GV oocytes and combined to form large structures in MII oocytes. The ELYSA forms a large spherical structure with tubular-vesicular structures approximately 2–10 μm in diameter and includes cytosolic components at the MII stage. After fertilization, ELYSA structures are gradually disassembled, and immature endosomes and lysosomes appear at the early 2-cell stages. The V1-subunit of vacuolar ATPase is recruited to these endosomes and lysosomes and causes further acidification of endosomal-lysosomal organelles, suggesting that the ELYSA maintains endosomal-lysosomal activity in a static state in oocytes for timely activation during early development.

35 **Introduction:**

36 Fertilization triggers the dynamic remodeling of cellular components via zygotic
37 gene expression following the degradation of the cellular components of each maternal and
38 paternal gamete. After fertilization, maternal cytosolic proteins and RNAs are selectively
39 degraded by the ubiquitin-proteasome system (UPS)[1] and specific RNA degradation
40 systems[2, 3], respectively. Treatment with a proteasome inhibitor or knockdown of the
41 zygote-specific proteasome assembly chaperone gene inhibits cytokinesis in zygotes,
42 suggesting an essential role for the UPS in early development[4, 5]. Membrane components
43 derived from each gamete are degraded by the lysosomal degradation system via autophagy
44 and endocytosis[6, 7]. In mice, autophagic activity is relatively low in meiosis II (MII) oocytes,
45 whereas it is rapidly upregulated approximately 4 h after fertilization, and LC3-positive
46 structures appear throughout the cytoplasm. Autophagic activity decreases slightly before
47 and after the 2-cell stage but remains high from the 4- to 8-cell stage[8]. Loss of Atg5 causes
48 embryonic lethality at the 4- to 8-cell stages, suggesting that autophagy is essential for early
49 mouse development. In contrast, some maternal plasma membrane (PM) proteins are
50 internalized from the PM at the late 2-cell stage and are selectively degraded by lysosomes[9].
51 Endocytosis inhibitors prevent cell division in 2-cell embryos, suggesting that endocytosis
52 plays a pivotal role in early development[9, 10]. Although lysosomal degradation systems are
53 drastically upregulated after fertilization, their regulation remains unknown.

54 In *Caenorhabditis elegans*, lysosomal activity in oocytes is upregulated by sperm-derived
55 factors as the oocytes grow and mature. In this process, translational arrest of mRNA
56 coding the V1-subunits of vacuolar ATPase in oocytes is released by the stimulation of

57 sperm-derived factors. As a result, the V1-subunits are recruited to the V0-subunits in the
58 lysosomal membrane, enhancing lysosomal acidification. This process is known as
59 lysosomal switching[11]. In mouse embryos, LysoTracker staining analysis suggests that
60 lysosomal acidification is prominent at the 2-cell stage but not in MII oocytes and zygotes[12],
61 raising the possibility that lysosomal switching takes place during mouse embryogenesis.

62 In this study, we aimed to investigate the dynamics of the endolysosomal system
63 during mouse oocyte maturation and embryogenesis. We found that endosomes and
64 lysosomes assembled to form spherical structures in germinal vesicle (GV)-stage oocytes,
65 which became larger as they matured into MII oocytes. Ultrastructural analysis showed that
66 these structures were large spherical membrane assemblies, including endosomes,
67 lysosomes, and tubulo-vesicular structures located in the periphery of the PM. We refer to
68 this structure as the Endosomal-LYSosomal organellar Assembly (ELYSA). The ELYSA
69 contains several cytosolic constituents. While ELYSAs are disassembled in late-stage
70 zygotes, immature endosomes and lysosomes gradually appear in the cytoplasm of early
71 2-cell stage embryos. Live imaging analysis showed that the V1-subunit of V-ATPase is
72 targeted to the endolysosomal membrane, resulting in further acidification of lysosomal
73 compartments during embryogenesis. These findings suggest that the ELYSA maintains
74 low endosomal and lysosomal activities and acts as a waiting place for endolysosomal
75 organelles to undergo fertilization-triggered activation toward embryogenesis.

76

77 **Results**

78 ***Endosomes and lysosomes coordinately form giant structures in MII oocytes***

79 To examine the localization of endosomes and lysosomes in mouse MII oocytes,
80 early or late endosomes were stained with anti-RAB5 or -RAB7 antibody, respectively, and
81 their localization was compared with that of lysosomes stained with anti-LAMP1 antibody.
82 Giant structures harboring lysosomes with early and late endosomes were detected (**Fig. 1A,**
83 **Supplementary Fig. 1, Supplementary Movie 1**). Each giant structure in the MII oocytes
84 was spherical, ellipsoidal, or concatenated with small spheres with short and long diameters
85 of 3–5 μm and up to 10 μm, respectively. These structures were located in the peripheral
86 region just beneath the PM, excluding the metaphase plate region in proximity to the
87 metaphase chromosomes. These structures were observed until the pronuclear-zygote
88 (PN-zygote) stage but were mostly disassembled at the 2-cell stage. The RAB5 and
89 LAMP1 signals separated after the first division, indicating that these giant structures were
90 transiently formed (**Fig. 1 B**).
91
92 ***Endosomes, lysosomes, and tubulo-vesicular structures form an ELYSA***
93 To clarify the internal structure of this giant structure containing lysosomes and
94 endosomes in the MII oocytes, we observed these in MII oocytes using correlative light and
95 electron microscopy (CLEM) using immunological reaction with anti-RAB7 and -LAMP
96 antibodies[13, 14]. RAB7- and LAMP1-signals were well detected even in the ultrathin section
97 (100 nm thickness) of the Epon-embedded MII oocyte, fixed with 0.025% glutaraldehyde
98 (GA), which showed similar distribution as shown in **Fig. 1** and **Supplementary Fig. 2**.
99 Toluidine blue staining in adjacent ultrathin section showed the RAB7/LAMP1-double
100 positive structures in the fluorescence observation were also positive for toluidine blue,

101 with interspaces were often found in the center of spheres (**Fig. 2A**). Confocal fluorescent
102 images in the ultrathin sections clarified that RAB7-positive signals were often observed on
103 the outside of these LAMP1-positive signals. Electron microscopic analysis of the
104 RAB7/LAMP-double positive region in the ultrathin section revealed that the
105 RAB7/LAMP1-dboule positive structures are assemblies of tubulo-vesicular structures, the
106 interior of that are either vacuolated or filled (**Fig. 2B**). The toluidine blue stain-positive
107 structures were confirmed to match in size and peripheral distribution with those identified
108 by RAB7/LAMP1 immunostaining, except for the metaphase plate, even under 2.5% GA
109 conditions for precise ultrastructural observation (**Supplementary Fig. 3, Supplementary**
110 **Movie 2**). Therefore, we examined the ultrastructural morphology of toluidine blue-positive
111 giant structures in MII oocytes fixed with 2.5% GA. The results showed that tubular
112 membrane vesicles with a short diameter of approximately 60.5 ± 15.9 nm assembled in the
113 structure, with gaps in the cytoplasm of approximately 24.0 ± 6.7 nm. Some of the vesicles
114 also harbored lysosome-like electron-dense contents, while others displayed multilamellar
115 or multivesicular body-like structures, whereas mitochondria appeared to be absent (**Fig.**
116 **2C**). Based on these observations, we termed this membrane assembly as the
117 Endosomal-LYSosomal organellar Assembly (ELYSA).
118
119 ***An autophagosome marker, LC3, also accumulated in ELYSA***
120 Decreased autophagic activity in MII oocytes is suggested by the fact that puncta
121 formation of transgenically expressed GFP-LC3, an autophagosome marker, disappeared at
122 the MII stage[8]. Since GFP fluorescence may be quenched under acidic conditions, we

examined the localization of LC3 in MII oocytes by immunostaining with an anti-LC3 antibody. We found that LC3 hardly formed puncta in the cytoplasm, but part of the LC3 signal overlapped with the ELYSA in MII oocytes (**Fig. 3A**), suggesting that LC3-positive membrane structures were also present in the ELYSA.

Immature ELYSA localizes in peripheral and perinuclear regions in preovulatory oocytes

We verified ELYSA formation in immature, preovulatory oocytes by performing immunostaining for LAMP1 with RAB5 or LC3 using mouse GV oocytes. We observed assemblies larger than 1 μm in GV oocytes, wherein fluorescent signals overlapped (**Fig. 4A,B**). The ELYSA at this stage was smaller than that in MII oocytes and was localized not only in the peripheral region of the PM but also in the vicinity of the GV nucleus.

ELYSA maturation proceeds actin dependently and may prevent V1 component access for vesicle acidification

Migration from the perinuclear to the peripheral region during oocyte maturation is similar to the redistribution of the endoplasmic reticulum (ER) and the formation of cortical ER clusters. Fitzharris et al. showed that the inhibition of actin cytoskeleton polymerization disturbs ER migration and cortical ER cluster formation[15]. Therefore, we added latrunculin A or cytochalasin B as inhibitors of actin polymerization and observed ELYSA formation after *in vitro* maturation (IVM) by immunostaining. While both drugs inhibited polar body extrusion and metaphase plate formation, as reported previously, these inhibitors reduced ELYSA size, as indicated by LAMP1, LC3, and RAB5 immunostaining, and caused the

145 redistribution of LAMP1-, LC3-, and RAB5-positive signals from the cell periphery to the
146 cytoplasm compared with control GV oocytes (**Fig. 5A**).

147 We then observed GV oocytes injected with LAMP1-EGFP and
148 ATP6V1A-mCherry mRNA (V1A-mCherry: a core component of V-ATPase in the
149 cytoplasm, which is associated with the outer lysosomal membrane during lysosomal
150 acidification). Live-cell imaging of LAMP1-EGFP fluorescence clearly captured the
151 ELYSA maturation dynamics during IVM and revealed that ELYSA size enlargement was
152 accelerated after germinal vesicle breakdown (GVBD, 2–3 h after IVM started) and that
153 ELYSA–ELYSA assembly occurred as ELYSAs migrated to the peripheral region (**Fig. 5B,**
154 **Supplementary Movie 3**). We also examined the expression of V1A-mCherry in oocytes
155 after IVM. V1A-mCherry was partly detected on the surface of the ELYSA in MII oocytes
156 but not significantly within the ELYSA (**Fig. 5C)**.

157

158 ***Acidification of lysosomes is initiated in coordination with ELYSA disassembly***

159 We examined the relationship between ELYSA disappearance and the emergence
160 of acidic membrane compartments during early development. LysoSensor probes exhibit
161 increased fluorescence in a pH-dependent manner upon acidification and enable the
162 semi-quantitative analysis of cellular acidic compartments, whereas LysoTracker probes
163 exhibit non-pH-dependent fluorescence. Thus, we costained oocytes and embryos at
164 various stages with LysoTracker Red and LysoSensor Green (in the same medium drop).
165 LysoTracker showed a pronounced puncta-like signal after the 2-cell stage, as previously
166 reported[12]. In contrast, the ELYSAs in GV and MII oocytes were clearly identified by

167 LysoSensor, whereas LysoTracker only produced a very dim ELYSA signal (**Fig. 6A**).

168 A comparison of LysoTracker and V1A-mCherry showed that these fluorescent
169 signals colocalized well on small bright vesicles but not on the ELYSA, and both
170 LysoTracker and V1A-mCherry puncta were reduced in embryos cultured in the presence
171 of bafilomycin A_1, which inhibits the H^+ translocation of V-ATPase (**Supplementary Fig.**
172 **4**). This suggests that LysoTracker detects membrane compartment acidification, but not
173 that in the ELYSA. In contrast, the LysoSensor results suggested that lysosomes in the
174 ELYSA were not neutralized and remained acidic at a lower level, even though V1A was
175 difficult to localize.

176 Live-cell imaging of embryos expressing V1A-mCherry in the presence of
177 LysoSensor was performed to examine the spatiotemporal relationship between V1A
178 localization and lysosomal acidification. Although the fluorescence of both signals was not
179 stably detected until the first 2–3 frames after the start of imaging, this method revealed that
180 the ELYSA disappeared or disassembled throughout the PN-zygote stage until the first
181 mitotic division. In addition, V1A accumulation was rarely observed in the PN-zygote stage
182 but was rapidly enhanced in the early 2-cell embryo stage. LysoSensor-positive punctate
183 structures, where V1A-mCherry accumulated, increased in number during the 2-cell stage
184 (**Fig. 6B, Supplementary Movie 4**).

185

186 ***Low-level cathepsin-dependent proteolytic activity was maintained in ELYSA***

187 Cathepsins are mainly responsible for the proteolytic activity in lysosomes. We
188 visualized the proteolytic activity of cathepsin B, the expression of which has been

189 confirmed in mouse embryos[12]. Mouse oocytes and embryos at various stages were
190 simultaneously collected and stained with Magic Red cathepsin B staining solution to
191 examine their relationship with the ELYSA. Magic Red staining showed that proteolytic
192 activity was detected not only in the small, isolated membrane structures (mature
193 lysosomes) but also in the ELYSA in the GV and MII oocytes, whereas small punctate
194 structures were predominantly stained in other stages (**Supplementary Fig. 5, Fig. 7A**).
195 The intensity plots of LysoSensor and Magic Red fluorescence revealed that the proteolytic
196 activity indicated by the Magic Red signal in the ELYSA was not as strong as that in
197 isolated punctate structures (lysosomes) in the GV and MII oocytes (**Fig. 7B**).
198

199 **Discussions:**

200 In this study, we identified a large spherical structure, the ELYSA, consisting of
201 endosomes, lysosomes, LC3-positive vesicles, and various vesicular-tubular structures in
202 mouse oocytes. ELYSAs appear in GV oocytes and become larger through assembly during
203 oocyte maturation. After fertilization, as ELYSAs gradually disassemble in zygotes, RAB5-,
204 RAB7-, or LAMP1-positive punctate structures appear in the cytoplasm of embryos at the
205 early 2-cell stage. The V1-subunit of V-ATPase is targeted to these structures, leading to
206 further acidification of the endosomal/lysosomal compartments. These results suggest that
207 the ELYSA functions as a reservoir that accumulates endosomal and lysosomal
208 compartments in the periphery of the cell cortex and maintains their activities in a static
209 state until embryogenesis following fertilization.

210 We previously found that some oocyte PM proteins are internalized from the PM at

211 the late 2-cell stage and are selectively degraded in lysosomes [9]. In this process, we noted
212 that lysosomes were not well stained by LysoTracker until the early 2-cell stage, but their
213 signals became stronger from the late 2-cell stage, suggesting the existence of a mechanism
214 underlying developmentally regulated endosomal/lysosomal activation during
215 embryogenesis [9, 12]. Notably, ELYSAs were stained with toluidine blue and LysoSensor,
216 suggesting that these structures were acidified to some extent. In addition, Magic Red,
217 which reflects cathepsin B activity, weakly stained ELYSAs. These observations indicate
218 that lysosomes in ELYSAs have some activity, albeit at low levels. Mouse oocytes
219 accumulate several maternal constituents, including proteins, lipids, and mRNA, and grow
220 to approximately 75 μm in diameter. In addition, oocytes must remain at the GV and MII
221 stages for an extended period to maintain their quality until fertilization. In such situations,
222 lysosomal degradation activity may be suppressed to a relatively low level by the ELYSA,
223 whereas nutrient uptake, storage, and protein synthesis are predominantly upregulated in
224 growing oocytes. Notably, the V1-subunits of V-ATPase were detected on the periphery of
225 ELYSAs but not in their interior. Thus, ELYSA formation may prevent V1-subunits from
226 targeting the lysosomal membrane inside the ELYSA.

227 Ultrastructural analysis revealed that the ELYSA consists of outer and inner
228 membrane assembly layers that contain several endosomes and lysosomes, respectively
229 (**Fig. 1, 2**). Upon disassembly of the ELYSA, endosomes in the outer layer and lysosomes
230 in the inner layer are expected to be released from the ELISA earlier and later, respectively.
231 This may explain the time lag between fertilization and lysosomal acidification beginning
232 at the early-2-cell stage. Since the ELYSA seems to contain cytosolic constituents, it may

233 accommodate some cytosolic constituents as a capsule to provide nutrition or signaling
234 factors for development.

235 Since the distance between membrane structures in the ELYSA appears to be
236 relatively uniform, cytoplasmic components in the ELYSA may contain factors that
237 promote membrane structure tethering or assembly. In fact, we observed that the cytoplasm
238 between the membrane structures inside the ELYSA had a slightly higher electron density.
239 In the future, identifying the cytoplasmic molecules tethering these membrane structures to
240 the ELYSA will be necessary.

241 We also found that ELYSAs were gradually distributed from the perinuclear region
242 to the periphery of the oocyte cell cortex, except in the MII cell plate, from the GV to the
243 MII stage. This movement is reminiscent of that of the ER and cortical ER clusters, whose
244 distribution is regulated by the actomyosin system[15]. In fact, actin cytoskeleton
245 polymerization inhibitors resulted in a reduced size of ELYSAs and their redistribution
246 from the cell cortex to the cytoplasm (**Fig. 5**), suggesting that the actin cytoskeleton is
247 involved in the formation and distribution of ELYSAs in oocytes.

248 Autophagy and endocytosis are upregulated in zygotes and 2-cell stage embryos,
249 respectively, and their substrates are delivered to the lysosomes for degradation. Our study
250 showed that lysosomal acidification was enhanced from the 2- to 4-cell stage and after the
251 morula stage. The first lysosomal acidification occurred when ELYSAs were disassembled
252 in late zygotes. These findings suggest that the timing of degradative substrate delivery to
253 lysosomes is developmentally linked to lysosomal acidification and maturation. Notably,
254 minor and major zygotic gene activation occurs at the 1- and 2-cell stages, respectively,

255 during mouse development, implying that lysosomal degradation of maternal components
256 is coupled with zygotic gene expression to promote embryogenesis[16]. Fertilization appears
257 to trigger ELYSA disassembly, but the downstream signaling pathway remains to be
258 identified and needs to be studied in the future.

259 Recently, it has been reported that appropriate lysosomal activity is important for
260 mammalian development[10]. Bafilomycin A_1 treatment arrests embryonic development at the
261 4–8-cell stage[12]. Inhibition of cathepsin activity using a mixture of E64d and pepstatin A
262 blocks the development of the 8-cell or morula stage[12]. However, autophagic activity in
263 fertilized eggs and embryonic developmental potential are correlated. Using GFP-LC3 as
264 an indicator of autophagic activity, Tsukamoto et al. found that aged eggs from 14- to
265 15-month-old mice had lower autophagic activity than those from younger mice, probably
266 due to decreased lysosomal activity. Females transplanted with embryos with high
267 autophagic activity have a significantly higher litter size ratio than that of control females[17].
268 Analysis of ELYSA formation and disassembly in aged oocytes and embryos may be a
269 useful tool for determining oocyte quality by examining whether appropriate regulation of
270 endosomal/lysosomal activities occurs.

271

272 **Methods:**

273 ***Animal experiments and strains***

274 Neither randomization nor blinding was used for animal selection (8–16-week-old). All
275 experimental protocols involving animals were approved and performed in accordance with
276 the guidelines of the Animal Care and Experimentation Committee of Gunma University

277 (Approval No. 22-076). Hybrid B6D2F1 mice were purchased from the Japan SLC
278 (Hamamatsu, Japan)
279
280 ***Antibodies and inhibitors***
281 The following primary antibodies were used: rabbit monoclonal anti-RAB5 (C8B1; 3547;
282 Cell Signaling Technology, Danvers, MA, USA), rabbit monoclonal anti-RAB7 (D95F2;
283 9367; Cell Signaling Technology), rat monoclonal anti-mouse LAMP1 (1D4B; sc-19992;
284 Santa Cruz Biotechnology, Dallas, TX, USA), and mouse monoclonal anti-rat LC3 (Clones
285 4E12; M152-3; Medical and Biological Laboratories, Tokyo, Japan). The following
286 secondary antibodies were used: goat anti-rabbit IgG (H+L) conjugated with Alexa Fluor
287 555 (A-21428; Thermo Fisher Scientific, Waltham, MA, USA), goat anti-rat IgG (H+L)
288 cross-adsorbed secondary antibody conjugated with Alexa Fluor 488 and 647 (A-11006 and
289 A-21247, respectively; Thermo Fisher Scientific), and goat anti-mouse IgG (H+L)
290 cross-adsorbed secondary antibody conjugated with Alexa Fluor 546 (A-11030; Thermo
291 Fisher Scientific). The following inhibitors or solutions were used for IVM or embryonic
292 culture assays: dimethyl sulfoxide (DMSO) (13406-55; Nacalai Tesque, Kyoto, Japan);
293 latrunculin A actin polymerization inhibitor that binds to monomer actin (428021;
294 Sigma-Aldrich, St. Louis, MO, USA); and cytochalasin B, an actin polymerization inhibitor
295 that binds to the plus-end of polymerized actin (C6762; Sigma-Aldrich). Stock solutions of
296 latrunculin A or cytochalasin B were prepared by solubilizing each in DMSO at 400×
297 concentration for assay. Bafilomycin A_1 was dissolved in DMSO (L266; Dojindo,
298 Kumamoto, Japan) at a final concentration of 25 nM.

299

300 ***Oocyte preparation***

301 GV oocytes were collected from the ovaries of female mice 46 h after injection with
302 pregnant mare serum gonadotropin or an anti-inhibin antibody (CARD HyperOva; Kyudo,
303 Kumamoto, Japan). Antral follicles were suspended in 30 μL of FHM medium drops
304 (Sigma-Aldrich) covered with liquid paraffin (Nacalai Tesque), punctured using 26G
305 needles (Terumo, Tokyo, Japan), and the GV oocytes were collected using a glass needle
306 with a mouth pipette. MII oocytes were collected from the oviducts of female mice 13 h
307 after injection with CARD HyperOva and 7.5 IU human chorionic gonadotropin (hCG;
308 ASKA Pharmaceutical, Tokyo, Japan) 48 h apart. The oviductal wall was punctured using a
309 26G needle to collect cumulus-oocyte complexes in 20 μL potassium simplex optimization
310 medium (KSOM; Kyudo) drops covered with liquid paraffin.

311

312 ***DNA vector construction and mRNA synthesis***

313 Complementary DNA for mouse *Lamp1* (accession number NM_001317353) or *Atp6v1a*
314 (accession number NM_001358204) was amplified using PCR with High-fidelity Taq
315 Polymerase, KOD FX Neo (Toyobo, Osaka, Japan), and a mouse ovary cDNA library as a
316 template (Genostaff, Tokyo, Japan). The amplicon was then subcloned into the entry vector
317 pDONR221, and transferred into the destination vectors pDEST-CMV-C-EGFP (#122844;
318 for *Lamp1*; Addgene, Watertown, MA, USA) or pDest-mCherry-N1 (#31907; for *Atp6v1a*;
319 Addgene) using Gateway recombination cloning technology. The following primer
320 combinations were used for the constructions:

321 5′-GCGCACAAGTTTGTACAAAAAAGCAGGCTGCCACCATGGCGGCCCCCGGCG-
322 3′ and
323 5′-GCGCACCACTTTGTACAAGAAAGCTGGGTTGTCTTCAAGGCTACGGAATG-3′
324 (for *Lamp1*), or
325 5′-GCGCACCACTTTGTACAAGAAAGCTGGGTTGATGGTCTGATAGCCGGCGTGA
326 CT-3′ and
327 5′-GCGCACCACTTTGTACAAGAAAGCTGGGTTGTCTTCAAGGCTACGGAATG-3′
328 (for *Atp6v1a*). The cDNA encoding *Lamp1-EGFP* or *Atp6v1a-mCherry* were amplified
329 using the following primer combinations: 5′-CGCAAATGGGCGGTAGGCGTG-3′ and
330 5′-TCCAGCAGGACCATGTGATCGC-3′ (for *Lamp1-EGFP*), or
331 5′-CGCAAATGGGCGGTAGGCGTG-3′ and 5′-TTGGTCACCTTCAGCTTGG-3′ (for
332 *Atp6v1a-mCherry*). RNA synthesis using each PCR amplicon as a template, poly-A tail
333 addition, and mRNA purification were performed, using an mMESSAGE mMACHINE T7
334 Ultra kit (Thermo Fisher Scientific) and MEGAclear transcription clean-up kit (Thermo
335 Fisher Scientific), according to the manufacturer's protocols. Synthesized mRNAs were
336 dissolved in RNase-free demineralized water at a concentration of 400 ng/μL and frozen in
337 aliquots until use.
338
339 **In vitro *maturation, fertilization, and embryonic culture***
340 IVM for the GV oocytes was conducted by washing the oocytes twice and culturing in
341 alpha-modified Eagle's minimum essential medium (Thermo Fisher Scientific) containing
342 5% (vol/vol) fetal bovine serum (FBS), 0.1 of IU/mL follicle-stimulating hormone (MSD,

343 Tokyo, Japan), 1.2 IU/mL of hCG (ASKA Pharmaceutical), and 4 ng/mL of epidermal
344 growth factor (Thermo Fisher Scientific) for 17 h at 37 °C under a 5% CO_2 atmosphere[18].
345 For *in vitro* fertilization, spermatozoa from a B6D2F1 epididymis were pre-incubated in a
346 100-μL modified human tubal fluid medium (Kyudo) drop covered with liquid paraffin and
347 inseminated at a sperm concentration of 1.5×10^5 per mL for 1.5 h. Excess spermatozoa
348 were washed out, and the oocytes were incubated in a 20-μL KSOM drop (Kyudo) for
349 further development. IVM assays using latrunculin A and cytochalasin B were performed
350 by transferring oocytes to medium drops containing each inhibitor or DMSO 4 h after the
351 start of IVM (waiting for the completion of GVBD), as previously reported[15]. IVM media
352 containing DMSO, latrunculin A, or cytochalasin B was prepared by diluting the stock
353 solution (1:400), and the final concentration of the inhibitors was 10 μM. The embryonic
354 culture assay using bafilomycin A_1 was conducted by transferring the PN-zygote into a
355 20-μL drop of KSOM containing 25 nM bafilomycin A_1 covered with liquid paraffin at 6 h
356 post-fertilization (hpf). Embryos were transferred at 24, 48, and 72 hpf to freshly prepared
357 KSOM containing bafilomycin A_1.
358
359 ***Immunostaining***
360 Immunostaining of oocytes or embryos was performed as previously described [9]. Oocytes
361 or embryos were cultured to the indicated stages and fixed in 4% paraformaldehyde (PFA;
362 Nacalai Tesque) in phosphate-buffered saline (PBS) containing 0.1 mg/mL polyvinyl
363 alcohol (PVA; Sigma-Aldrich) (PVA/PBS) for 15 min at 25–27 °C. After fixation, the cells
364 were permeabilized with PVA/PBS containing 0.1% Triton X-100 (Sigma-Aldrich) for 30

365 min at 25–27 °C and washed thrice with PVA/PBS. After blocking with 10% FBS (Thermo
366 Fisher Scientific) in PBS for 1 h at room temperature, the cells were incubated with the
367 aforementioned primary antibodies (1:100 for all) overnight at 4 °C. Next, the cells were
368 washed thrice in PVA/PBS, and incubated with anti-mouse, rat, or rabbit IgG secondary
369 antibodies coupled with Alexa Fluor 488, 555, or 564 (1:200 for all; Thermo Fisher
370 Scientific) at 25–27 °C for 2–4 h. Thereafter, the cells were incubated with PVA/PBS
371 containing 10 μg/mL Hoechst 33342 (Dojindo) for 10 min and washed with fresh PVA/PBS
372 a few times. Subsequently, control and nonspecific staining were performed by processing
373 oocytes and embryos in the absence of primary antibodies. The oocytes and embryos were
374 imaged in PVA/PBS microdrops in 35-mm glass-bottomed dishes (MatTek Corporation,
375 Ashland, MA, USA). For each position, confocal images at 81 *z*-axis planes with 1-μm
376 increments were acquired on an IX-71 inverted microscope (Olympus Corporation, Tokyo,
377 Japan) equipped with a CSU W-1 confocal scanner unit (Yokogawa Electric Corporation)
378 using a 60× silicone immersion lens (Olympus Corporation).
379
380 ***LysoTracker/LysoSensor staining of oocytes at various stages***
381 Acidic organelles in the oocytes were visualized using LysoTracker Red DND-99 and
382 LysoSensor Green DND-189 (Thermo Fisher Scientific) according to the manufacturer's
383 instructions. Briefly, the oocytes or embryos at target stages for one experimental round
384 were obtained simultaneously and incubated in a large drop of reaction mixture (KSOM
385 containing 1/10,000 Magic Red stock solution dissolved in DMSO and 1/1,000 LysoSensor
386 Green DND-189 stock solution dissolved in DMSO) for 30 min at 37 °C under 5% CO_2 in

387 a humidified atmosphere in liquid paraffin in a 35-mm glass-bottom dish (MatTek
388 Corporation). Subsequently, confocal images at 41 *z*-axis planes with 2-μm increments
389 were obtained using a CSU W-1 spinning disk confocal microscope with a 30× silicone
390 immersion lens.
391
392 ***Magic Red/LysoSensor staining***
393 Intracellular cathepsin activity was assayed in oocytes or embryos using Magic Red
394 Cathepsin B or Cathepsin L detection kits (ImmunoChemistry Technologies LLC, Davies,
395 CA, USA) according to the manufacturer's instructions. Briefly, the oocytes or embryos at
396 target stages for one experimental round were obtained simultaneously and incubated in a
397 large drop of reaction mixture (KSOM containing 1/250 Magic Red stock solution
398 dissolved in DMSO and 1/1,000 LysoSensor Green DND-189 stock solution dissolved in
399 DMSO) for 25 min at 37 °C under 5% CO_2 in a humidified atmosphere in liquid paraffin in
400 a 35-mm glass-bottom dish (MatTek Corporation). Afterward, Hoechst 33342 (10 μg/mL)
401 was added to the drop to be a final concentration of 10 μg/mL, and incubated for a further 5
402 min. Subsequently, oocytes or embryos at the same stage were collected, and confocal
403 images at 41 *z*-axis planes with 2-μm increments for both 470-nm (LysoSensor) and
404 555-nm (Magic Red) lasers were obtained on a CSU W-1 spinning disk confocal
405 microscopy using a 30× silicone immersion lens.
406
407 ***In-resin CLEM and electron microscopy***
408 In-resin CLEM was performed as previously described with some modifications[13, 14].

409 Briefly, oocytes were fixed in 4% PFA and 0.025% glutaraldehyde (GA). After
410 permeabilization with 50 μg/mL digitonin (Nacalai Tesque) and 0.02% Triton X-100,
411 oocytes were washed with PVA/PBS three times and incubated with PBS containing 10%
412 (w/v) FBS (Thermo Fisher Scientific) for 1 h at room temperature. Thereafter, oocytes were
413 incubated with PVA/PBS containing primary antibody overnight at 4 °C. After incubation
414 with a secondary antibody in PVA/PBS for 2 h, oocytes were fixed in 4% PFA and 2.5%
415 GA, embedded in 1.5% agarose, stained with osmium tetroxide, dehydrated with graded
416 ethanol solutions (QY1), and embedded in epoxy resin (Oken Shoji, Tokyo, Japan).
417 Ultrathin sections of Epon-embedded oocytes (100-nm thickness) were prepared using a
418 Leica UC6 ultramicrotome (Leica, Nussloch, Germany) and placed on glass coverslips.
419 Subsequently, fluorescence microscopy images of the sections were obtained using a Nikon
420 A1RHD25 confocal laser scanning microscope with a NIS-Elements software (Nikon,
421 Tokyo, Japan). Electron microscopic images were observed using a Helios Nanolab 660
422 FIB-SEM instrument (FEI Company, Hillsboro, USA).
423 For conventional electron microscopy, the oocytes were fixed in the presence of 2% PFA
424 and 2.5% GA and stained with osmium tetroxide. After dehydration with ethanol, the
425 oocytes were embedded in epoxy resin, as described above. Sections were cut at a thickness
426 of 100 nm using a UC6 ultramicrotome, mounted on glass coverslips, stained with uranyl
427 acetate and lead citrate, and observed under a Regulus8240 scanning electron microscope
428 (Hitachi High-Tech Corporation, Tokyo, Japan).
429
430 ***Serial semi-thin sections and 3D reconstruction of toluidine blue-positive structures***

431 Serial semi-thin sections were cut at a thickness of 300 nm using a UC6 ultramicrotome
432 and mounted on glass slides. Next, the sections were stained with 1% toluidine blue/0.1 M
433 PB, and images were obtained using a BX50 light microscope (Olympus Corporation).
434 Serial toluidine blue-stained images were aligned using FIJI (National Institutes of Health,
435 MD, USA) with plugin-linear stack alignment using SIFT (LSAS), and 3D reconstruction
436 was performed using Amira software (Thermo Fisher Scientific).
437
438 ***Microinjection into the oocytes***
439 Microinjection of mRNA into GV oocytes was performed as previously described[19, 20].
440 Briefly, antral follicles were harvested in FHM medium containing 250 μM of dbcAMP
441 using 26G needles (Terumo). After dissociating the cumulus cells by pipetting, the oocytes
442 were transferred to medium supplemented with 250 μM of dbcAMP and 10 μM of
443 cytochalasin B (Sigma-Aldrich). Thereafter, mRNA injection into the oocytes was
444 performed using a piezo-micromanipulator (Primetech, Tokyo, Japan) with a glass capillary
445 needle. The mRNA concentrations were 50 and 100 ng/μL for *V1A-mCherry* and
446 *Lamp1-EGFP*, respectively. The oocytes were washed thrice and used for IVM. mRNA was
447 microinjected into MII oocytes as previously described. The concentration of mRNA was
448 the same as that in the GV oocytes.
449
450 ***Time-lapse confocal imaging of oocytes/embryos***
451 Low-invasive confocal fluorescence imaging of oocytes/embryos was performed as
452 previously described[21, 22, 23] with slight modifications. Briefly, on an inverted microscope

453 IX-71 (Olympus Corporation) equipped with a CSU W-1 confocal scanner unit (Yokogawa
454 Electric Corporation), an incubation chamber (Tokai Hit, Fujinomiya, Japan) was set at
455 37 °C on the microscope stage, with a gas mixture of 5% CO_2 introduced into the chamber
456 at 150 mL/min. Oocytes/embryos were placed in 8 μL of IVM medium or KSOM drops
457 covered with liquid paraffin (Nacalai Tesque) in 35-mm glass-bottomed dishes (MatTek
458 Corporation). Subsequently, confocal images at 41 *z*-axis planes with 2-μm increments for
459 excitation lasers of 470 and 555 nm from an LDI-7 Laser Diode Illuminator (89North,
460 Williston, VT, USA) were obtained every 30 or 60 min during IVM or embryonic culture
461 observation, respectively, through optimized band-pass filters using 30× silicone immersion
462 lens.
463
464 ***Imaging analysis***
465 Analysis of the acquired images, including the generation of a line plot of intensity,
466 adjustment of intensity, and generation of montage images at a uniform intensity, was
467 performed using ImageJ software (National Institutes of Health). To enhance the images, a
468 Gaussian Blur filter (at a sigma radius of 1) and auto-adjustment of the intensity were
469 applied to the stack of images. To adjust the intensity, auto-adjustment of the intensity was
470 applied to each image. The movies were concatenated using Premiere Pro software (Adobe,
471 San Jose, CA, USA).
472
473 **Data availability:**
474 The data supporting the findings of this study are available from the corresponding authors

upon request.

Materials availability statement:

The materials supporting the findings of this manuscript are available from the corresponding authors upon reasonable request.

Acknowledgments:

We would like to thank Editage (www.editage.jp) for the English language editing.

Funding:

This study was supported by the Japan Society for the Promotion of Science KAKENHI (Grant Numbers 19H05711 and 20H00466 to K. Sato, 21H02435, 22H02872, and 22H04652 to I. Tanida, and 20K22744 to J. Yamaguchi), the Mochida Memorial Foundation for Medical and Pharmaceutical Research, Takeda Science Foundation (Grant Number 2022093867), and The Cell Science Research Foundation to Y. Satouh. This work was partly supported by the Project for Elucidating and Controlling Mechanisms of Aging and Longevity from the Japan Agency for Medical Research and Development (AMED 21gm5010003 to Y. Uchiyama., 22gm1710001 s0201 and 23gm1710001s0202 to I. Tanida) and by the MEXT-supported Program for the Strategic Research Foundation at Private Universities (to Y. Uchiyama), and the Center of Genomic and Regeneration Medicine, Juntendo University Graduate School of Medicine (to Y. Uchiyama and I. Tanida).

Competing interests:

No competing interests declared.

Author contributions:

Y.S. and K.S. established the essential research concepts for this study. Y.S. and T.T. performed the immunostaining and assays using mouse oocytes/embryos. I. T., J. Y., and Y. U. performed the CLEM experiments and analyses. Y. S. and K. S. mainly prepared the manuscript.

References:

1. Verlhac MH, Terret ME, Pintard L. Control of the oocyte-to-embryo transition by the ubiquitin-proteolytic system in mouse and *C. elegans*. *Curr Opin Cell Biol* **22**, 758-763 (2010).

2. Jiang ZY, Fan HY. Five questions toward mRNA degradation in oocytes and preimplantation embryos: when, who, to whom, how, and why? *Biol Reprod* **107**, 62-75 (2022).

3. Schier AF. The maternal-zygotic transition: death and birth of RNAs. *Science* **316**, 406-407 (2007).

4. Shin SW*, et al.* Mouse zygote-specific proteasome assembly chaperone important

519 for maternal-to-zygotic transition. *Biol Open* **2**, 170-182 (2013).

520

521 5. Shin SW*, et al.* Inhibition of the ubiquitin-proteasome system leads to delay of the

522 onset of ZGA gene expression. *J Reprod Dev* **56**, 655-663 (2010).

523

524 6. Sato K. Multiple roles of endocytosis and autophagy in intracellular remodeling

525 during oocyte-to-embryo transition. *Proc Jpn Acad Ser B Phys Biol Sci* **98**, 207-221

526 (2022).

527

528 7. Birgisdottir AB, Johansen T. Autophagy and endocytosis - interconnections and

529 interdependencies. *J Cell Sci* **133**, (2020).

530

531 8. Tsukamoto S, Kuma A, Murakami M, Kishi C, Yamamoto A, Mizushima N.

532 Autophagy is essential for preimplantation development of mouse embryos. *Science*

533 **321**, 117-120 (2008).

534

535 9. Morita A, Satouh Y, Kosako H, Kobayashi H, Iwase A, Sato K. Clathrin-mediated

536 endocytosis is essential for the selective degradation of maternal membrane proteins

537 and preimplantation development. *Development* **148**, dev199461 (2021).

538

539 10. Satouh Y, Sato K. Reorganization, specialization, and degradation of oocyte

540 maternal components for early development. *Reprod Med Biol* **22**, e12505 (2023).

541

542 11. Bohnert KA, Kenyon C. A lysosomal switch triggers proteostasis renewal in the
543 immortal *C. elegans* germ lineage. *Nature* **551**, 629-633 (2017).
544

545 12. Tsukamoto S*, et al.* Functional analysis of lysosomes during mouse preimplantation
546 embryo development. *J Reprod Dev* **59**, 33-39 (2013).
547

548 13. Tanida I, Yamaguchi J, Suzuki C, Kakuta S, Uchiyama Y. Application of immuno-
549 and affinity labeling with fluorescent dyes to in-resin CLEM of Epon-embedded
550 cells. *Heliyon* **9**, e17394 (2023).
551

552 14. Mitsui S, Yamaguchi J, Suzuki C, Uchiyama Y, Tanida I. TUNEL-positive structures
553 in activated microglia and SQSTM1/p62-positive structures in activated astrocytes
554 in the neurodegenerative brain of a CLN10 mouse model. *Glia* **71**, 2753-2769
555 (2023).
556

557 15. FitzHarris G, Marangos P, Carroll J. Changes in endoplasmic reticulum structure
558 during mouse oocyte maturation are controlled by the cytoskeleton and cytoplasmic
559 dynein. *Dev Biol* **305**, 133-144 (2007).
560

561 16. Schulz KN, Harrison MM. Mechanisms regulating zygotic genome activation. *Nat*
562 *Rev Genet* **20**, 221-234 (2019).

563

564 17. Tsukamoto S*, et al.* Fluorescence-based visualization of autophagic activity predicts
565 mouse embryo viability. *Sci Rep* **4**, 4533 (2014).
566

567 18. Morohaku K*, et al.* Complete in vitro generation of fertile oocytes from mouse
568 primordial germ cells. *Proc Natl Acad Sci U S A* **113**, 9021-9026 (2016).
569

570 19. Umeda R*, et al.* Structural insights into tetraspanin CD9 function. *Nat Commun* **11**,
571 1606 (2020).
572

573 20. Kato K*, et al.* Structural and functional insights into IZUMO1 recognition by JUNO
574 in mammalian fertilization. *Nat Commun* **7**, 12198 (2016).
575

576 21. Nozawa K, Satouh Y, Fujimoto T, Oji A, Ikawa M. Sperm-borne phospholipase C
577 zeta-1 ensures monospermic fertilization in mice. *Sci Rep* **8**, 1315 (2018).
578

579 22. Satouh Y, Nozawa K, Yamagata K, Fujimoto T, Ikawa M. Viable offspring after
580 imaging of Ca2+ oscillations and visualization of the cortical reaction in mouse
581 eggs. *Biol Reprod* **96**, 563-575 (2017).
582

583 23. Satouh Y, Inoue N, Ikawa M, Okabe M. Visualization of the moment of mouse
584 sperm-egg fusion and dynamic localization of IZUMO1. *J Cell Sci* **125**, 4985-4990

585 (2012).

586

587 **Figure legends:**

588 **Fig. 1. Endosomes and lysosomes form giant structures in the periphery of the oocyte**
589 **plasma membrane.**

590 (A) Meiosis II (MII) oocytes were fixed and costained with anti-RAB5 and anti-LAMP1
591 antibodies. The schematic diagram indicates the location of oocyte chromosomes and
592 metaphase plate in the MII oocytes. Maximum intensity projection of confocal images of
593 80-μm in height are shown as Z-projection images. Arrowheads indicate the positions of
594 oocyte chromosomes. Magnified regions (right) are indicated by yellow boxes. DNA was
595 stained with Hoechst 33342. (B) Embryos at different stages were fixed and costained with
596 anti-RAB5 and anti-LAMP1 antibodies. Hour(s) post-fertilization is indicated as hpf.

597

598 **Fig. 2. Endosomal-lysosomal organelles form assembly structures (ELYSA).**

599 (A) The internal structure of the giant structure in MII oocytes was analyzed by correlative
600 light and electron microscopy (CLEM) analysis using anti-RAB7 and anti-LAMP1
601 antibodies. A merged image of immunostaining and electron microscopy (EM) is indicated
602 (left), and a toluidine blue staining image of the adjacent thin section (right) is indicated.
603 Black arrowheads indicate the giant structures positive for the RAB7/LAMP1/toluidine
604 blue stainings. Note that RAB7/LAMP1 staining is indicated in a pseudo-color. (B) The
605 fluorescent distribution of RAB7/LAMP1 immunostaining was analyzed with
606 deconvolution confocal microscopy. Note that RAB7/LAMP1 staining is indicated in

607 pseudo-color. (C) The internal structures of the toluidine blue-positive structure, ELYSA,
608 were observed using conventional electron microscopy of oocytes fixed with 2.5%
609 glutaraldehyde. Magnified regions in a or b (right) are indicated by boxes (left). Arrows,
610 arrowheads, or asterisks indicate vesicles harboring high electron density contents and
611 multilamellar or multivesicular structures, respectively. ELYSA, endosomal lysosomal
612 organellar assembly.
613
614 **Fig. 3. An autophagy marker LC3 is also detected in ELYSA.**
615 MII oocytes were fixed and costained with anti-LC3 and anti-LAMP1 antibodies. The
616 maximum intensity projection of the confocal images of 80-μm in height is shown as a
617 Z-projection image. Magnified regions (right) are indicated by yellow boxes. DNA was
618 stained with Hoechst 33342. Arrowheads indicate the positions of oocyte chromosomes.
619
620 **Fig. 4. ELYSA grows and migrates to the peripheral region during oocyte maturation.**
621 Germinal vesicle oocytes were fixed and costained with anti-RAB5 and anti-LAMP1
622 antibodies (A) or anti-LC3 and anti-LAMP1 antibodies (B). The maximum intensity
623 projection of the confocal images of 80-μm in height is shown as a Z-projection image.
624 Magnified perinuclear regions (right) are indicated by yellow boxes. DNA was stained with
625 Hoechst 33342.
626
627 **Fig. 5. Enlargement of ELYSA and its redistribution to the cell periphery occur in an**
628 **actin cytoskeleton-dependent manner.**

629 (A) GV oocytes, after *in vitro* maturation (IVM) treatment with or without actin
630 polymerization inhibitors (10 μM latrunculin A or cytochalasin B), were fixed and
631 costained with anti-LC3 and anti-LAMP1 antibodies. Maximum intensity projection of
632 confocal images of 80-μm in height are shown as Z-projection images. DNA was stained
633 with Hoechst 33342. Arrowheads or asterisks indicate the metaphase plate or first polar
634 body, respectively. (B) EGFP fluorescence of GV oocytes injected with *Lamp1-EGFP* and
635 *V1A-mCherry* mRNA was analyzed using time-lapse imaging. Maximum intensity
636 projection of confocal images of 40-μm in height (bottom half of the oocyte) are shown.
637 Magnified perinuclear regions (right) are indicated by yellow boxes. Arrowheads indicate
638 assemblies that adhere to each other in the subsequent frame. (C) The same oocyte in (B)
639 after IVM. Maximum intensity projection of confocal images for both EGFP and mCherry
640 fluorescence of 80-μm in height are shown. Magnified regions in a or b (right) are indicated
641 by yellow boxes.
642
643 **Fig. 6. Endosomes and lysosomes in the ELYSA are acidified weakly, but further**
644 **acidification occurs after ELYSA disassembly.**
645 (A) Oocytes and embryos at different stages were stained in the same drop for LysoSensor
646 Green and LysoTracker Red staining analysis, and confocal images were acquired. (B)
647 Green and red fluorescence of pronuclear oocytes injected with *V1A-mCherry* mRNA was
648 analyzed using time-lapse imaging in the presence of LysoSensor Green to the blastocyst
649 stage. Magnified perinuclear regions are indicated by yellow boxes. Maximum intensity
650 projection of confocal images of 80-μm in height are shown unless otherwise stated.

651

652 **Fig. 7. Proteolytic activity of cathepsin B is maintained relatively at a low level in the**
653 **ELYSA.**

654 (A) GV and MII oocytes were stained in the same drop for LysoSensor Green and Magic
655 Red cathepsin B staining analysis, and confocal images were acquired. (B) Fluorescent
656 intensities of LysoSensor and Magic Red on the yellow lines indicated in (A) are indicated
657 by a line plot. Small, filled dots indicate the origin (0 μm) in distance.

658

659 **Supplementary Fig. 1. Endosomes and lysosomes form giant structures in the**
660 **periphery of the oocyte plasma membrane.**

661 (A) MII oocytes were fixed and costained with anti-RAB7 and anti-LAMP1 antibodies.
662 The schematic diagram indicates the location of oocyte chromosomes and the metaphase
663 plate in the MII oocytes. Maximum intensity projection of confocal images of 80-μm in
664 height are shown as Z-projection images. Arrowheads indicate the positions of oocyte
665 chromosomes.

666

667 **Supplementary Fig. 2. Giant structures in MII oocytes were immunostained with**
668 **anti-RAB7 and LAMP1 antibodies after glutaraldehyde (GA) fixation.**

669 (A) MII oocytes were fixed with 0.025% GA and costained with anti-RAB5/RAB7 and
670 anti-LAMP1 antibodies. Single-section images from confocal observation are indicated.

671

672 **Supplementary Fig. 3. Toluidine blue-positive structures in MII oocytes show similar**

673 **localization patterns to the ELYSA.**

674 (A) Aligned serial toluidine blue-stained light microscopic images were stacked and
675 three-dimensionally reconstructed by inversing the intensity and adjusting it to be
676 transparent. (B) A series of images of toluidine blue-stained serial semi-thin sections of the
677 Epon-embedded MII oocyte were reconstructed to 3D. Based on the images obtained,
678 chromosomes were segmented blue, toluidine blue-positive structures were segmented
679 yellow, and oocyte PM was segmented white.

680

681 **Supplementary Fig. 4. LysoTracker-positive punctate structures colocalized with**
682 **V1A-mCherry.**

683 Green and red fluorescence images of embryos expressing V1A-mCherry (mRNA injected
684 at 3 h post-fertilization [hpf]) and stained with LysoTracker Green at the indicated time
685 points were acquired. The maximum intensity projection of confocal images of 80-μm in
686 height is indicated.

687

688 **Supplementary Fig. 5. Magic Red cathepsin B staining gave signals in the cytoplasm**
689 **as well as the ELYSA in GV and MII oocytes..**

690 Fluorescence images of oocytes and embryos at the indicated stages were obtained and
691 stained with Magic Red Cathepsin B solution (and LysoTracker Green; not shown) in the
692 same drop of medium. The average intensity projections of confocal images of 80-μm in
693 height are shown.

694

695 **Supplementary Movie 1.**

696 MII oocytes were fixed and costained with anti-RAB5 and anti-LAMP1 antibodies. A series
697 of the confocal images of 81 slices of 80-μm in height is shown from top to bottom.

698

699 **Supplementary Movie 2.**

700 A series of continuous toluidine blue-stained light microscopic images of same oocyte (top
701 half) reconstructed to 3D. Chromosomes in the images obtained were segmented blue,
702 toluidine blue-positive structures were segmented yellow, and oocyte PM was segmented
703 white.

704

705 **Supplementary Movie 3.**

706 Time-lapse movie of EGFP fluorescence in the GV oocytes injected with *Lamp1-EGFP* and
707 *V1A-mCherry* mRNA during IVM with a maximum intensity Z-projection of confocal
708 images of 80-μm in height. Magnified perinuclear regions in Fig. 5 are indicated by a box.
709 The timestamp indicates the time after IVM started.

710

711 **Supplementary Movie 4.**

712 Time-lapse movie of fertilized oocytes expressing V1A-mCherry mRNA in the presence of
713 LysoSensor Green during embryonic development. The maximum intensity projection of
714 confocal images of 80-μm in height is shown.

Figure 1

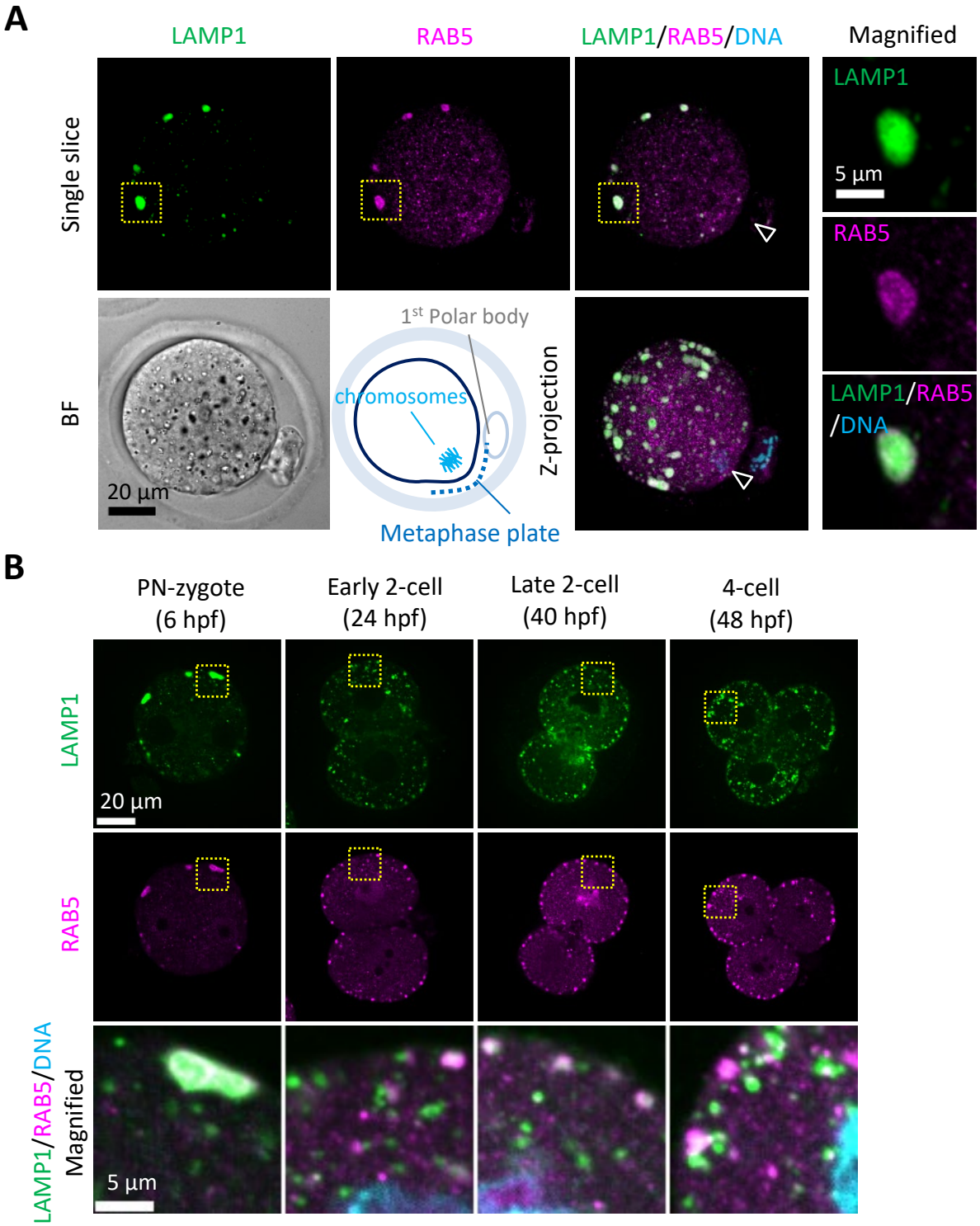

Fig. 1. Endosomes and lysosomes form giant structures in the periphery of the oocyte plasma membrane. (A) Meiosis II (MII) oocytes were fixed and costained with anti-RAB5 and anti-LAMP1 antibodies. The schematic diagram indicates the location of oocyte chromosomes and metaphase plate in the MII oocytes. Maximum intensity projection of confocal images of 80-µm in height are shown as Z-projection images. Arrowheads indicate the positions of oocyte chromosomes. Magnified regions (right) are indicated by yellow boxes. DNA was stained with Hoechst 33342. (B) Embryos at different stages were fixed and costained with anti-RAB5 and anti-LAMP1 antibodies. Hour(s) post-fertilization is indicated as hpf.

Figure 2

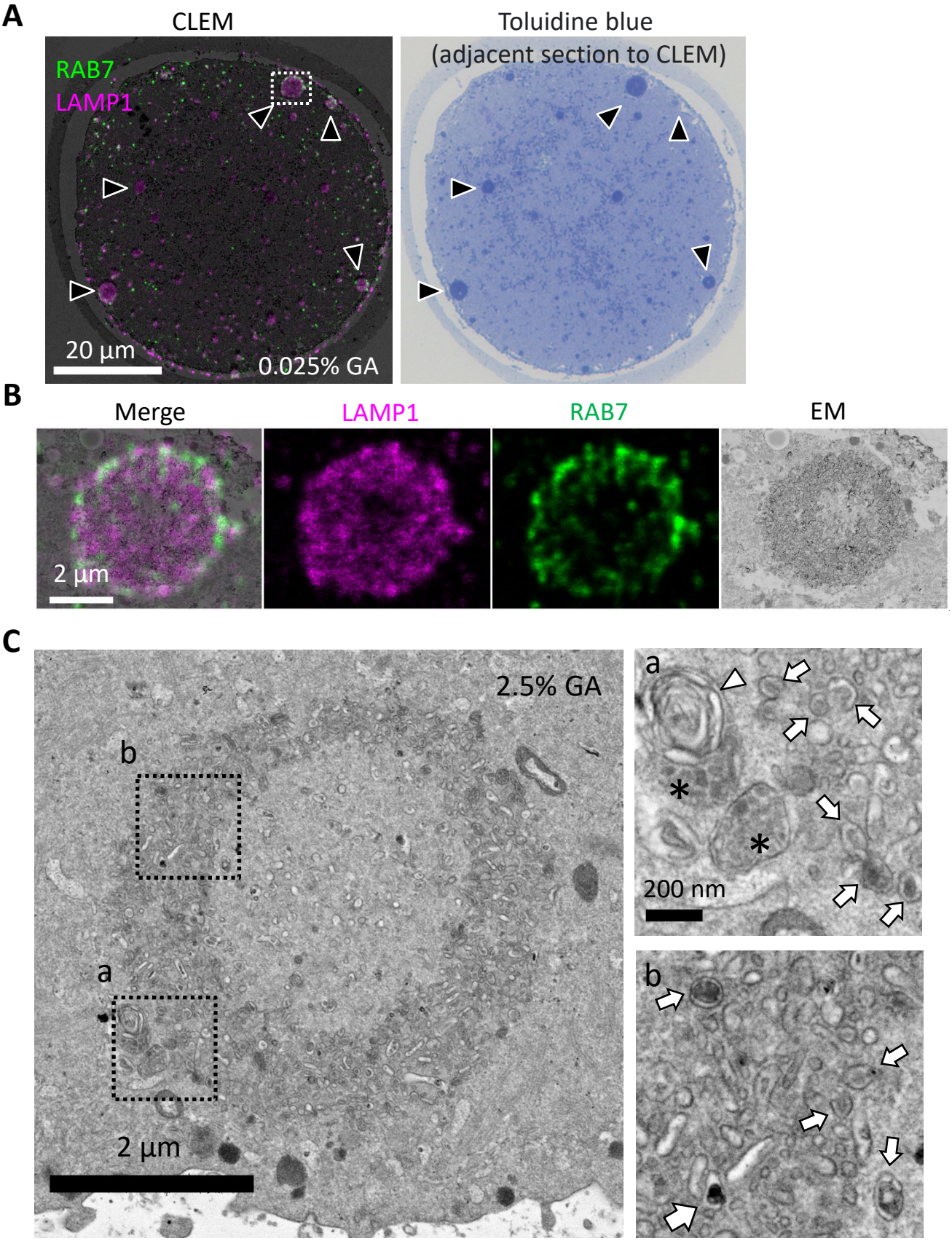
A
CLEM
Toluidine blue
(adjacent section to CLEM)
RAB7
LAMP1
20 µm
0.025% GA
B
Merge
LAMP1
RAB7
EM
2 µm
C
2.5% GA
b
a
2 µm
a
200 nm
b

Fig. 2. Endosomal-lysosomal organelles form assembly structures (ELYSA).
(A) The internal structure of the giant structure in MII oocytes was analyzed by correlative light and electron microscopy (CLEM) analysis using anti-RAB7 and anti-LAMP1 antibodies. A merged image of immunostaining and electron microscopy (EM) is indicated (left), and a toluidine blue staining image of the adjacent thin section (right) is indicated. Black arrowheads indicate the giant structures positive for the RAB7/LAMP1/toluidine blue stainings. Note that RAB7/LAMP1 staining is indicated in a pseudo-color. (B) The fluorescent distribution of RAB7/LAMP1 immunostaining was analyzed with deconvolution confocal microscopy. Note that RAB7/LAMP1 staining is indicated in pseudo-color. (C) The internal structures of the toluidine blue-positive structure, ELYSA, were observed using conventional electron microscopy of oocytes fixed with 2.5% glutaraldehyde. Magnified regions in a or b (right) are indicated by boxes (left). Arrows, arrowheads, or asterisks indicate vesicles harboring high electron density contents and multilamellar or multivesicular structures, respectively. ELYSA, endosomal lysosomal organellar assembly.

Figure 3

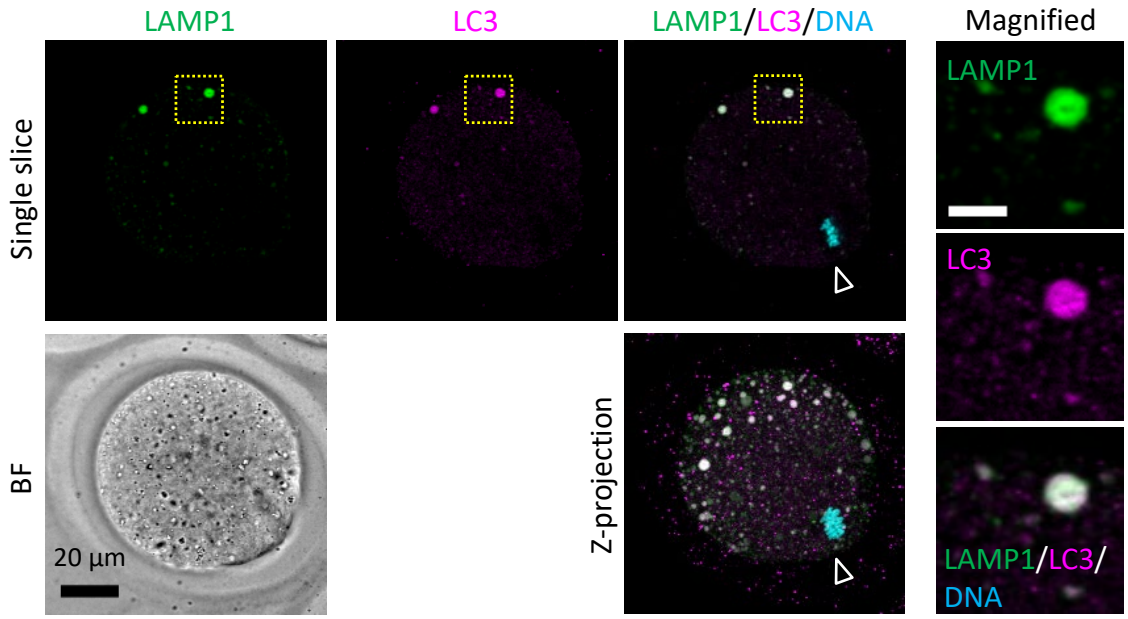

Fig. 3. An autophagy marker LC3 is also detected in ELYSA.
MII oocytes were fixed and costained with anti-LC3 and anti-LAMP1 antibodies. The maximum intensity projection of the confocal images of 80-µm in height is shown as a Z-projection image. Magnified regions (right) are indicated by yellow boxes. DNA was stained with Hoechst 33342. Arrowheads indicate the positions of oocyte chromosomes.

Figure 4

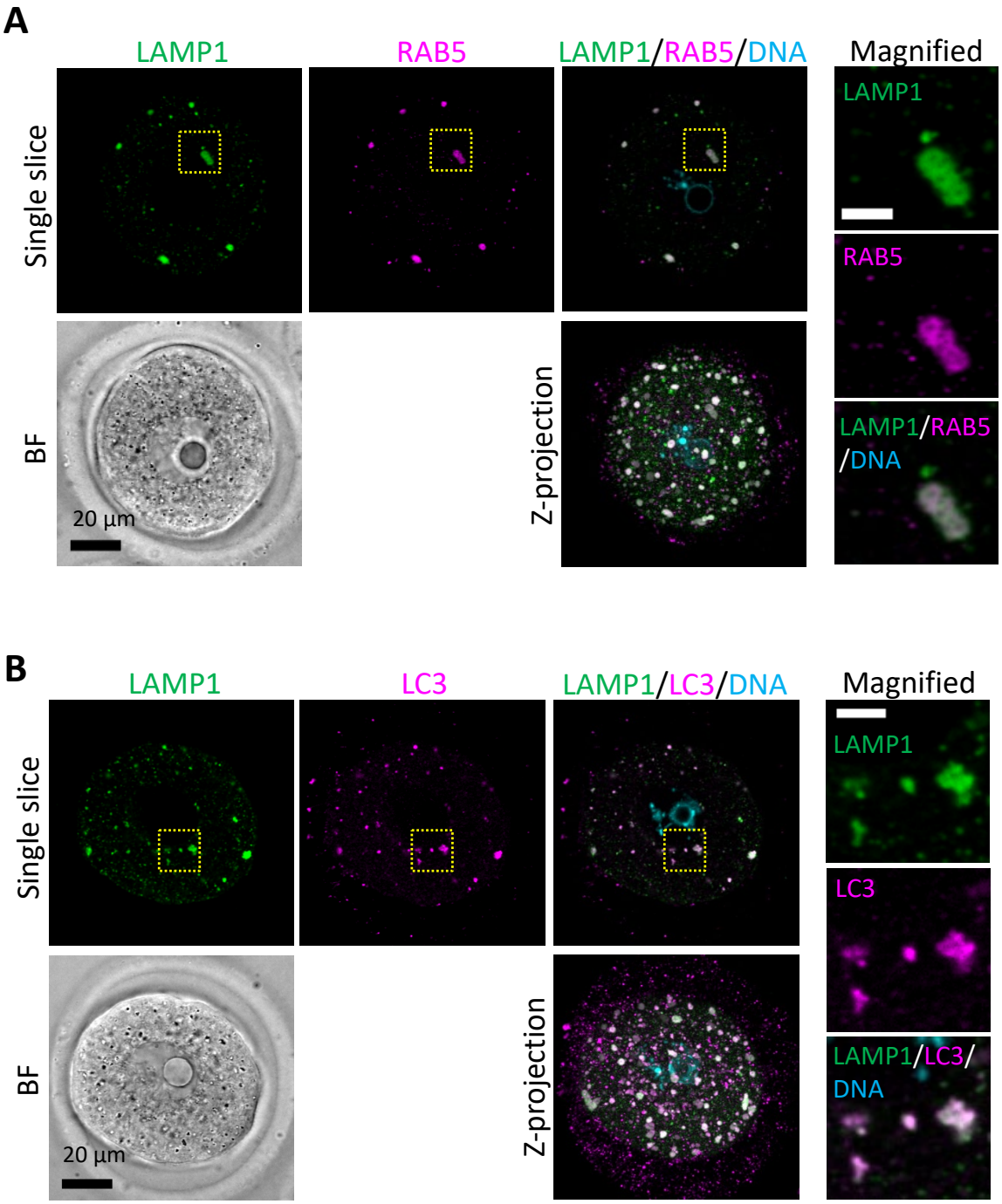

Fig. 4. ELYSA grows and migrates to the peripheral region during oocyte maturation. Germinal vesicle oocytes were fixed and costained with anti-RAB5 and anti-LAMP1 antibodies (A) or anti-LC3 and anti-LAMP1 antibodies (B). The maximum intensity projection of the confocal images of 80-µm in height is shown as a Z-projection image. Magnified perinuclear regions (right) are indicated by yellow boxes. DNA was stained with Hoechst 33342.

Figure 5

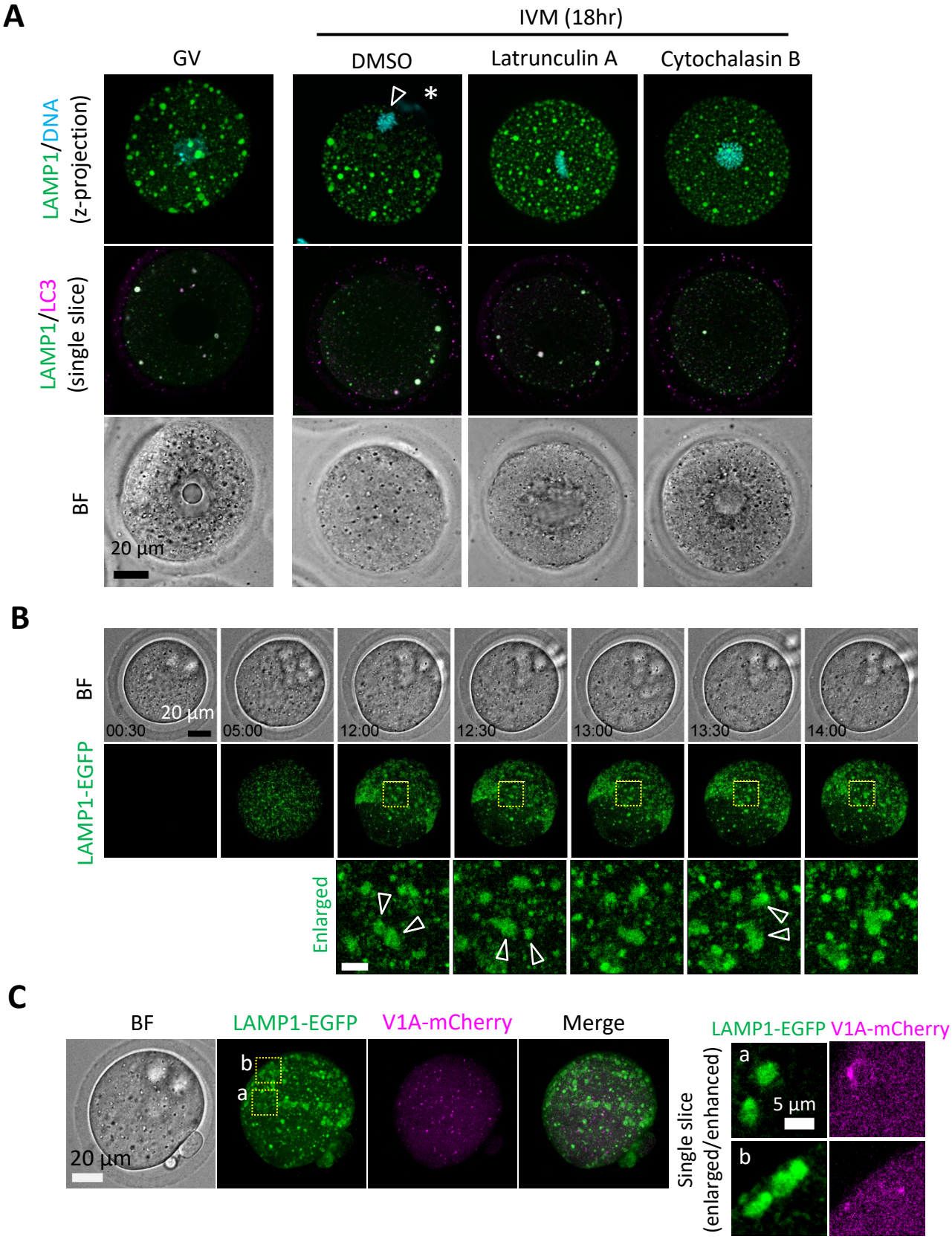
A
IVM (18hr)
GV
DMSO
Latrunculin A
Cytochalasin B
LAMP1/DNA (z-projection)
LAMP1/LC3 (single slice)
BF
20 µm
B
BF
20 µm
00:30
05:00
12:00
12:30
13:00
13:30
14:00
LAMP1-EGFP
Enlarged
C
BF
LAMP1-EGFP
V1A-mCherry
Merge
20 µm
b
a
LAMP1-EGFP V1A-mCherry
Single slice (enlarged/enhanced)
5 µm

Fig. 5. Enlargement of ELYSA and its redistribution to the cell periphery occur in an actin cytoskeleton-dependent manner.

(A) GV oocytes, after *in vitro* maturation (IVM) treatment with or without actin polymerization inhibitors (10 μM latrunculin A or cytochalasin B), were fixed and costained with anti-LC3 and anti-LAMP1 antibodies. Maximum intensity projection of confocal images of 80-μm in height are shown as Z-projection images. DNA was stained with Hoechst 33342. Arrowheads or asterisks indicate the metaphase plate or first polar body, respectively. (B) EGFP fluorescence of GV oocytes injected with *Lamp1-EGFP* and *V1A-mCherry* mRNA was analyzed using time-lapse imaging. Maximum intensity projection of confocal images of 40-μm in height (bottom half of the oocyte) are shown. Magnified perinuclear regions (right) are indicated by yellow boxes. Arrowheads indicate assemblies that adhere to each other in the subsequent frame. (C) The same oocyte in (B) after IVM. Maximum intensity projection of confocal images for both EGFP and mCherry fluorescence of 80-μm in height are shown. Magnified regions in a or b (right) are indicated by yellow boxes.

Figure 6

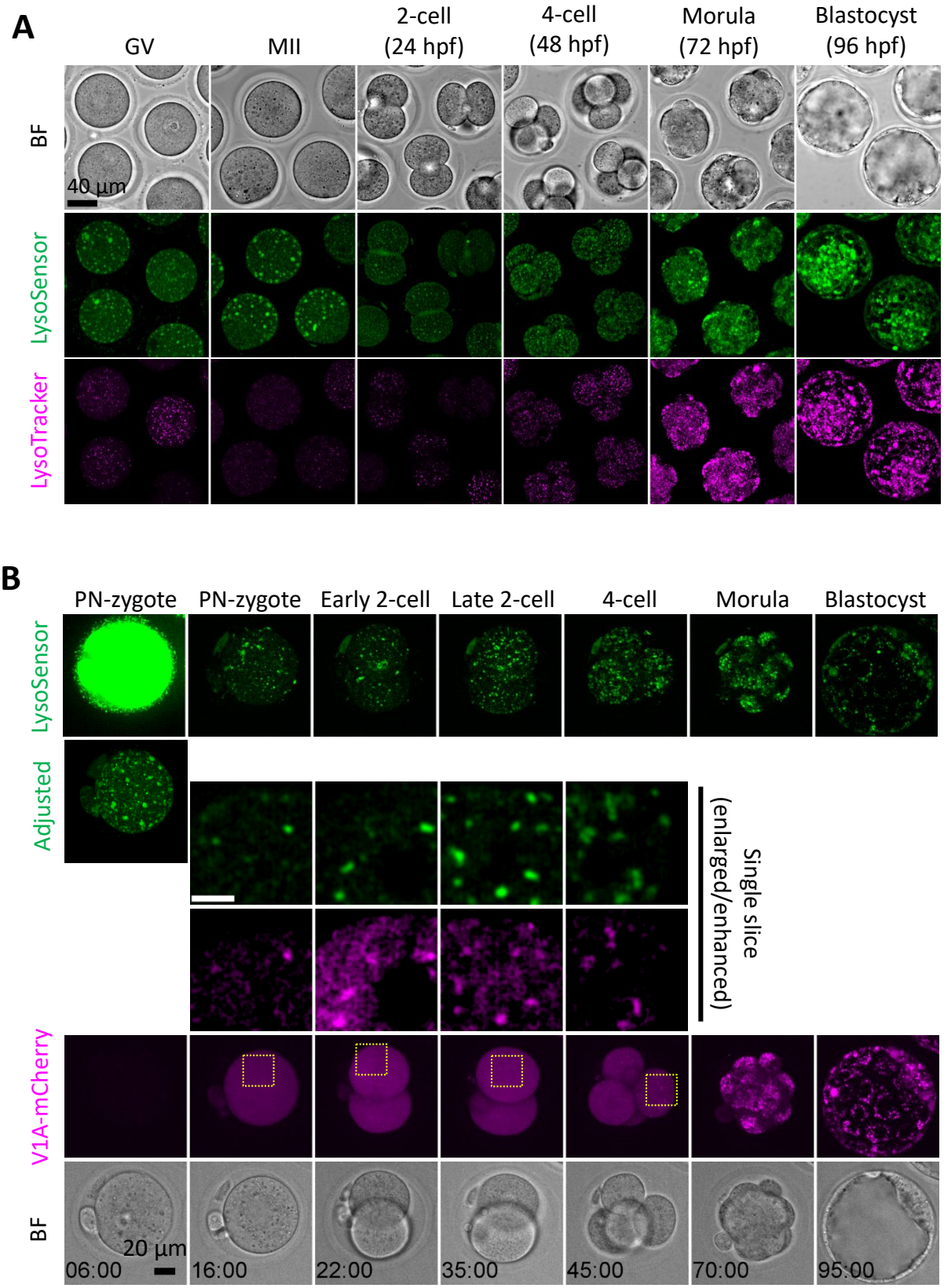
A
GV
MII
2-cell (24 hpf)
4-cell (48 hpf)
Morula (72 hpf)
Blastocyst (96 hpf)
BF
40 µm
LysoSensor
LysoTracker
B
PN-zygote
PN-zygote
Early 2-cell
Late 2-cell
4-cell
Morula
Blastocyst
LysoSensor
Adjusted
Single slice (enlarged/enhanced)
V1A-mCherry
BF
20 µm
06:00
16:00
22:00
35:00
45:00
70:00
95:00

Fig. 6. Endosomes and lysosomes in the ELYSA are acidified weakly, but further acidification occurs after ELYSA disassembly.

(A) Oocytes and embryos at different stages were stained in the same drop for LysoSensor Green and LysoTracker Red staining analysis, and confocal images were acquired. (B) Green and red fluorescence of pronuclear oocytes injected with *V1A-mCherry* mRNA was analyzed using time-lapse imaging in the presence of LysoSensor Green to the blastocyst stage. Magnified perinuclear regions are indicated by yellow boxes. Maximum intensity projection of confocal images of 80-μm in height are shown unless otherwise stated.

Figure 7

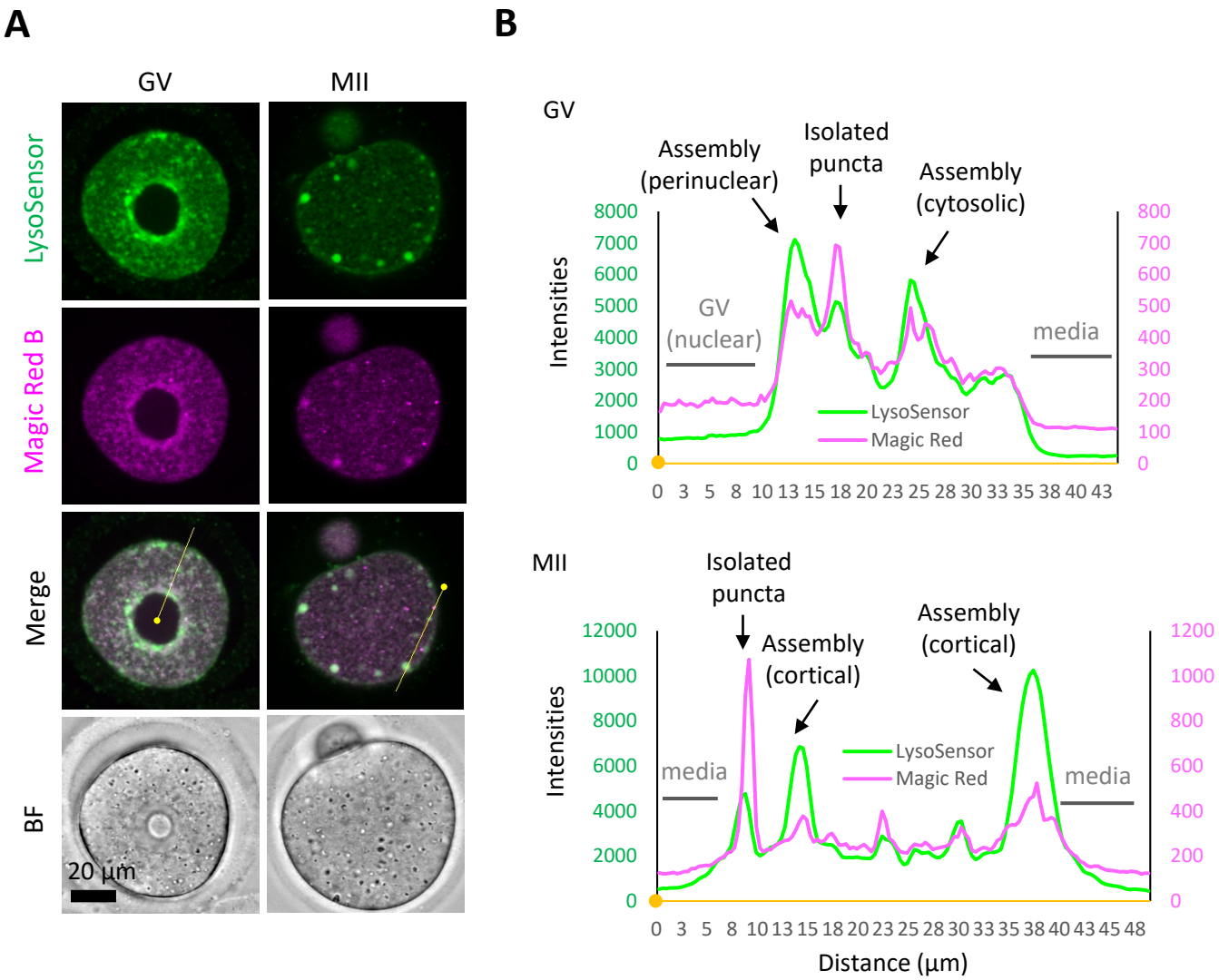

Fig. 7. Proteolytic activity of cathepsin B is maintained relatively at a low level in the ELYSA. (A) GV and MII oocytes were stained in the same drop for LysoSensor Green and Magic Red cathepsin B staining analysis, and confocal images were acquired. (B) Fluorescent intensities of LysoSensor and Magic Red on the yellow lines indicated in (A) are indicated by a line plot. Small, filled dots indicate the origin (0 µm) in distance.

Supplementary Figure 1

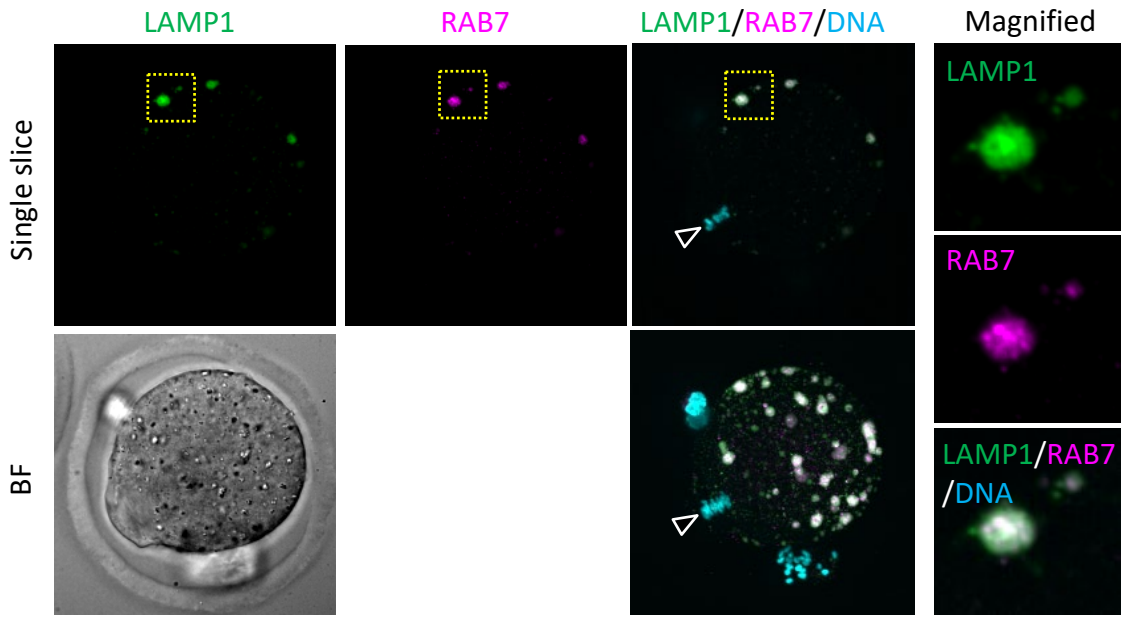

Supplementary Fig. 1. Endosomes and lysosomes form giant structures in the periphery of the oocyte plasma membrane.
(A) MII oocytes were fixed and costained with anti-RAB7 and anti-LAMP1 antibodies. The schematic diagram indicates the location of oocyte chromosomes and the metaphase plate in the MII oocytes. Maximum intensity projection of confocal images of 80-µm in height are shown as Z-projection images. Arrowheads indicate the positions of oocyte chromosomes.

Supplementary Figure 2

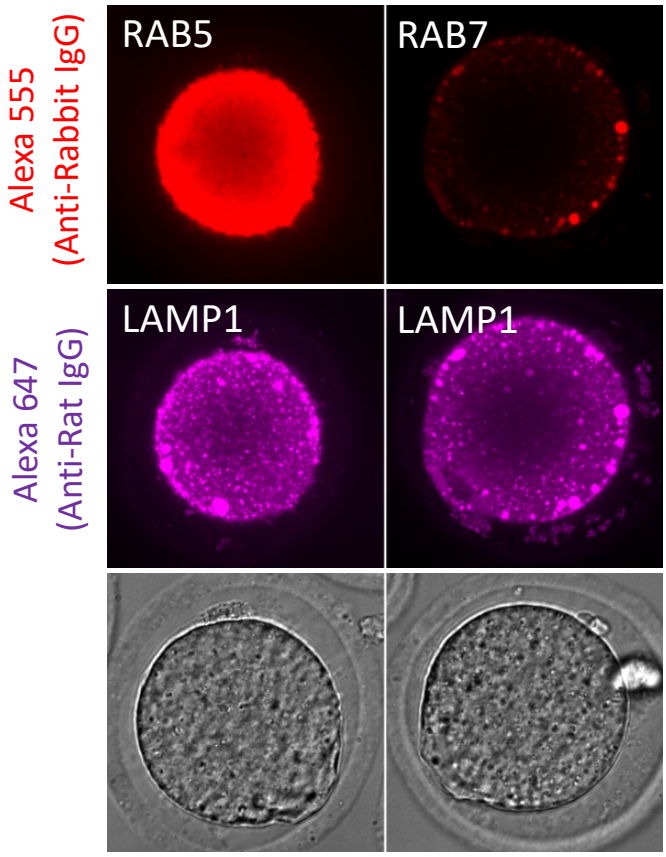

Supplementary Fig. 2. Giant structures in MII oocytes were immunostained with anti-RAB7 and LAMP1 antibodies after glutaraldehyde (GA) fixation.
(A) MII oocytes were fixed with 0.025% GA and costained with anti-RAB5/RAB7 and anti-LAMP1 antibodies. Single-section images from confocal observation are indicated.

Supplementary Figure 3

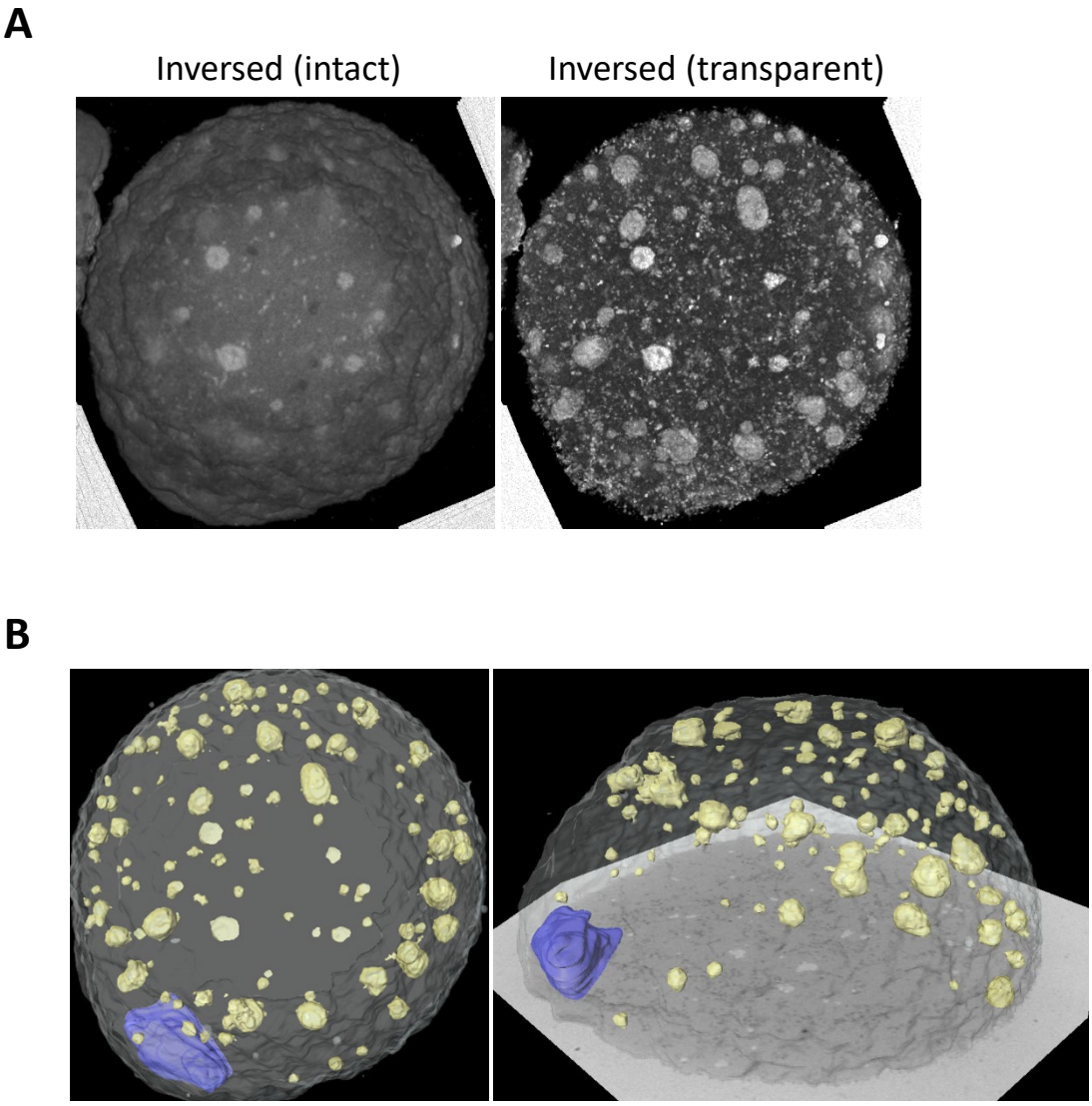

Supplementary Fig. 3. Toluidine blue-positive structures in MII oocytes show similar localization patterns to the ELYSA.
(A) Aligned serial toluidine blue-stained light microscopic images were stacked and three-dimensionally reconstructed by inversing the intensity and adjusting it to be transparent. (B) A series of images of toluidine blue-stained serial semi-thin sections of the Epon-embedded MII oocyte were reconstructed to 3D. Based on the images obtained, chromosomes were segmented blue, toluidine blue-positive structures were segmented yellow, and oocyte PM was segmented white.

Supplementary Figure 4

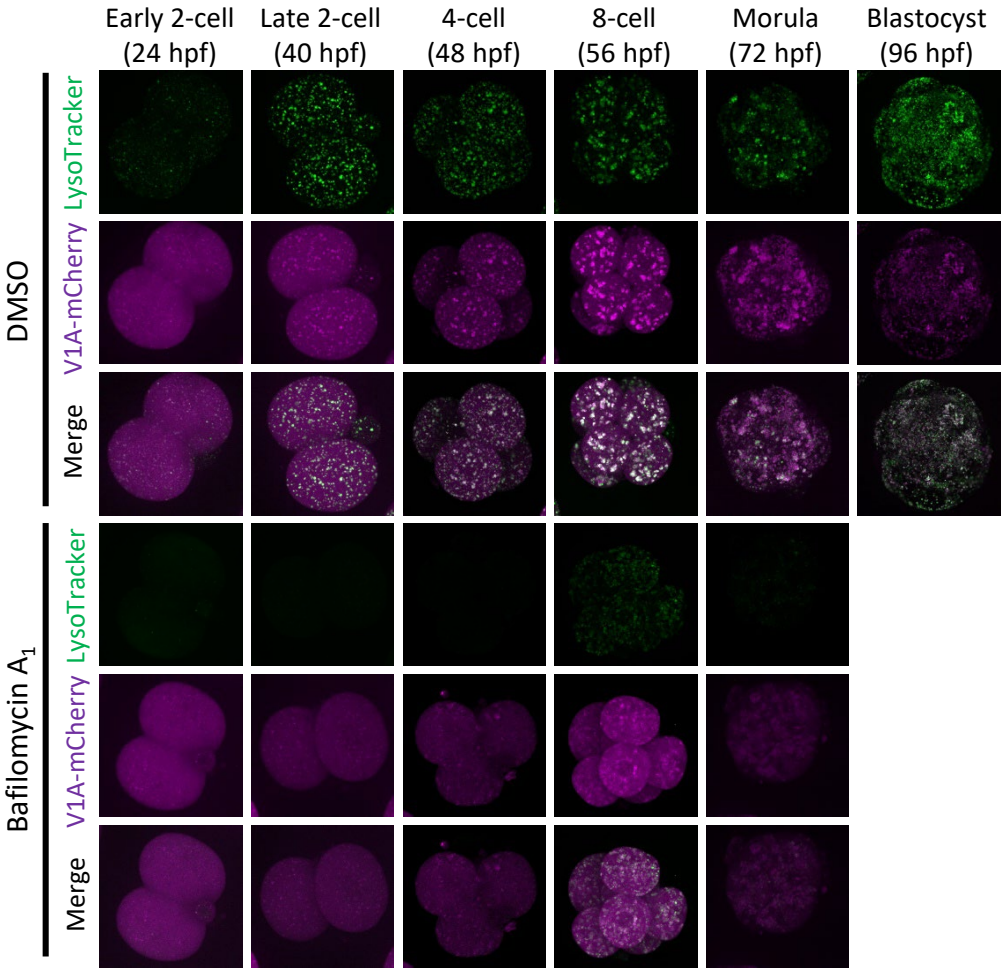

Supplementary Fig. 4. LysoTracker-positive punctate structures colocalized with V1A-mCherry. Green and red fluorescence images of embryos expressing V1A-mCherry (mRNA injected at 3 h post-fertilization [hpf]) and stained with LysoTracker Green at the indicated time points were acquired. The maximum intensity projection of confocal images of 80-μm in height is indicated.

Supplementary Figure 5

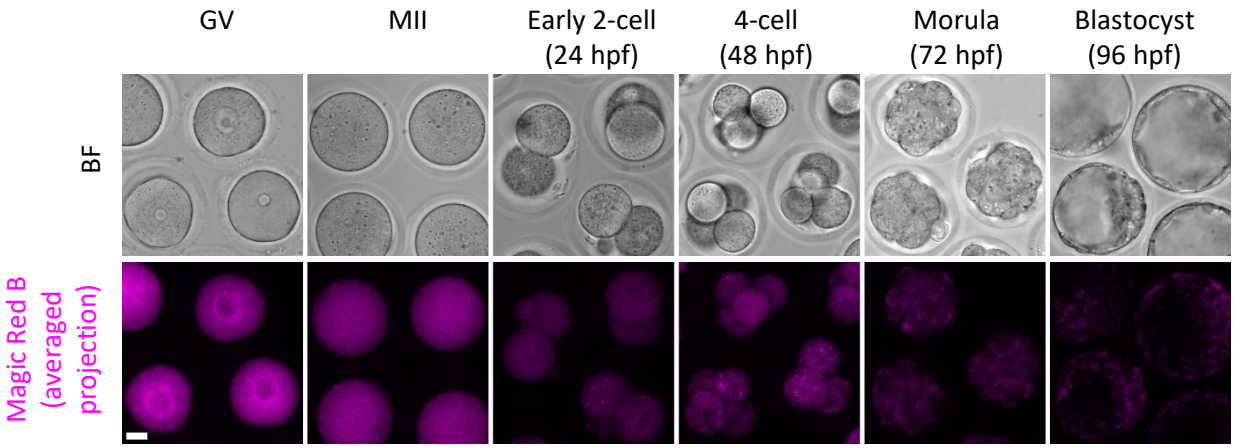

Supplementary Fig. 5. Magic Red cathepsin B staining gave signals in the cytoplasm as well as the ELYSA in GV and MII oocytes..
Fluorescence images of oocytes and embryos at the indicated stages were obtained and stained with Magic Red Cathepsin B solution (and LysoTracker Green; not shown) in the same drop of medium. The average intensity projections of confocal images of 80-μm in height are shown.

Supplementary Movie 1

Supplementary Movie 1.
MII oocytes were fixed and costained with anti-RAB5 and anti-LAMP1 antibodies. A series of the confocal images of 81 slices of 80-µm in height is shown from top to bottom.

Supplementary Movie 2

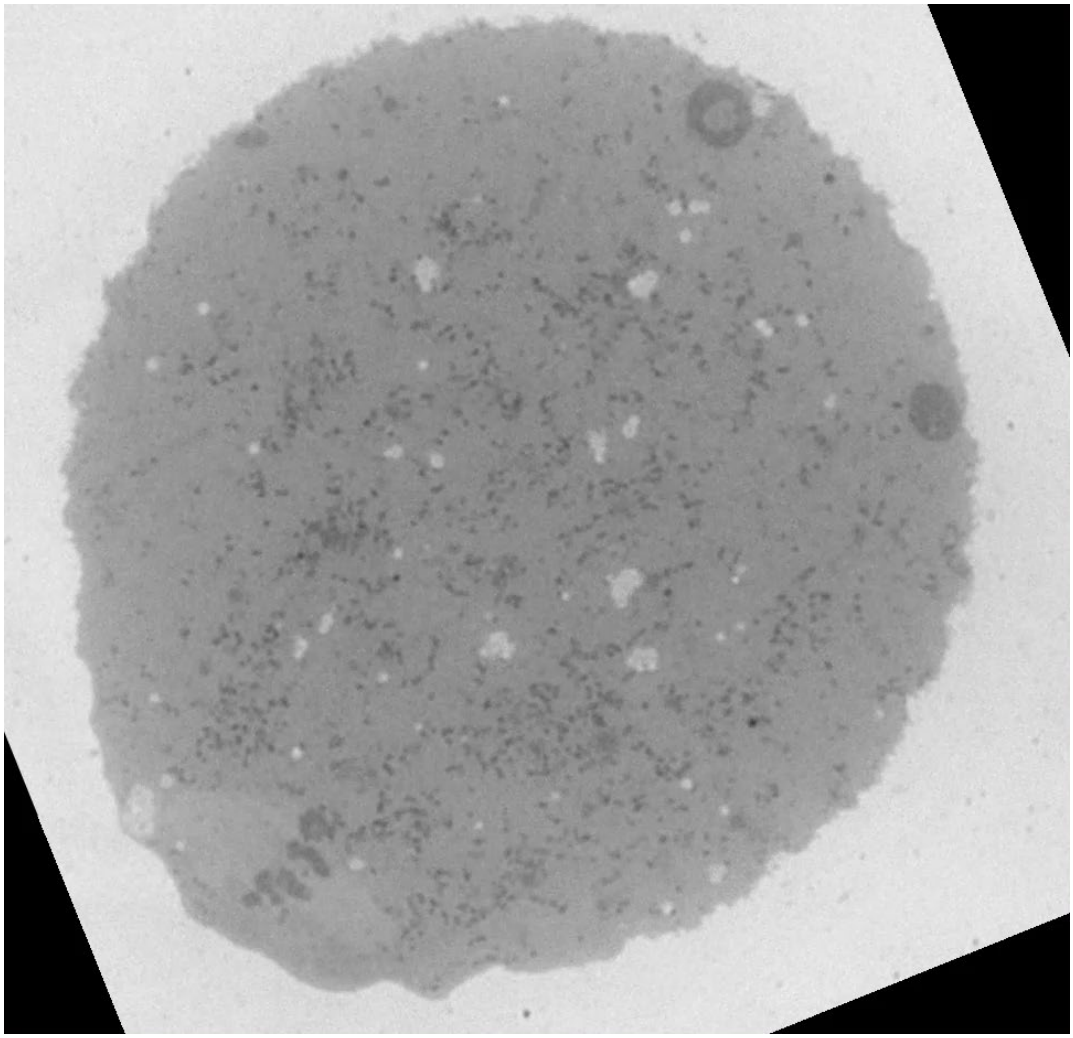

Supplementary Movie 2.
A series of continuous toluidine blue-stained light microscopic images of same oocyte (top half) reconstructed to 3D. Chromosomes in the images obtained were segmented blue, toluidine blue-positive structures were segmented yellow, and oocyte PM was segmented white.

Supplementary Movie 3

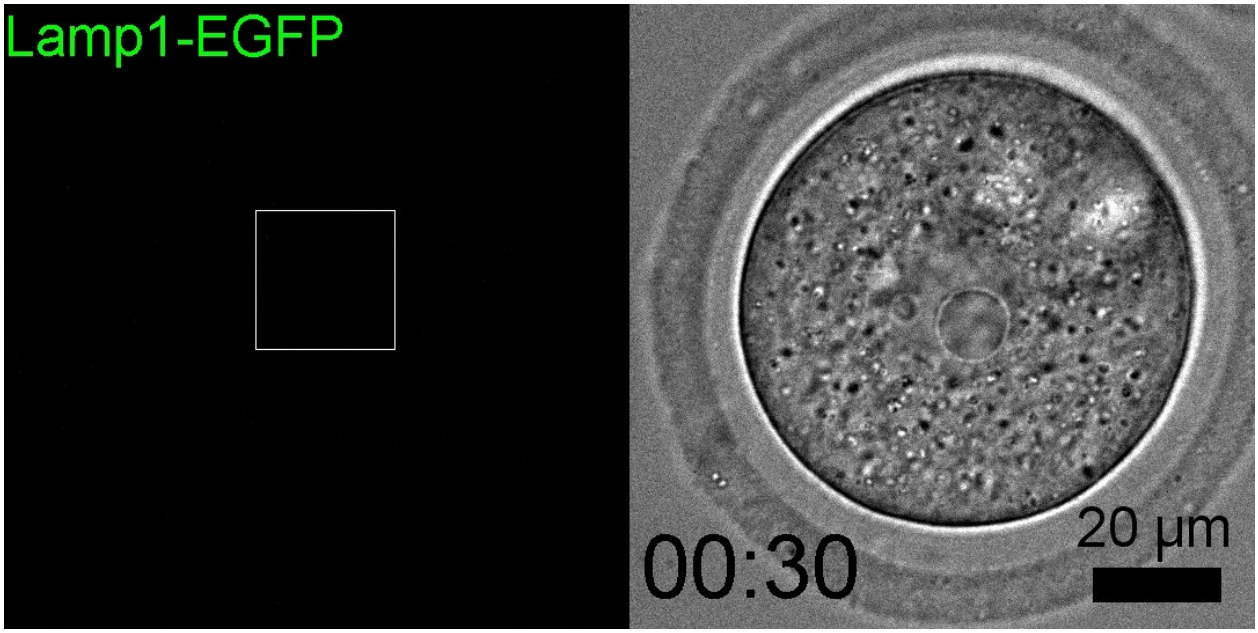

Supplementary Movie 3.
Time-lapse movie of EGFP fluorescence in the GV oocytes injected with *Lamp1-EGFP* and *V1A-mCherry* mRNA during IVM with a maximum intensity Z-projection of confocal images of 80-µm in height. Magnified perinuclear regions in Fig. 5 are indicated by a box. The timestamp indicates the time after IVM started.

Supplementary Movie 4

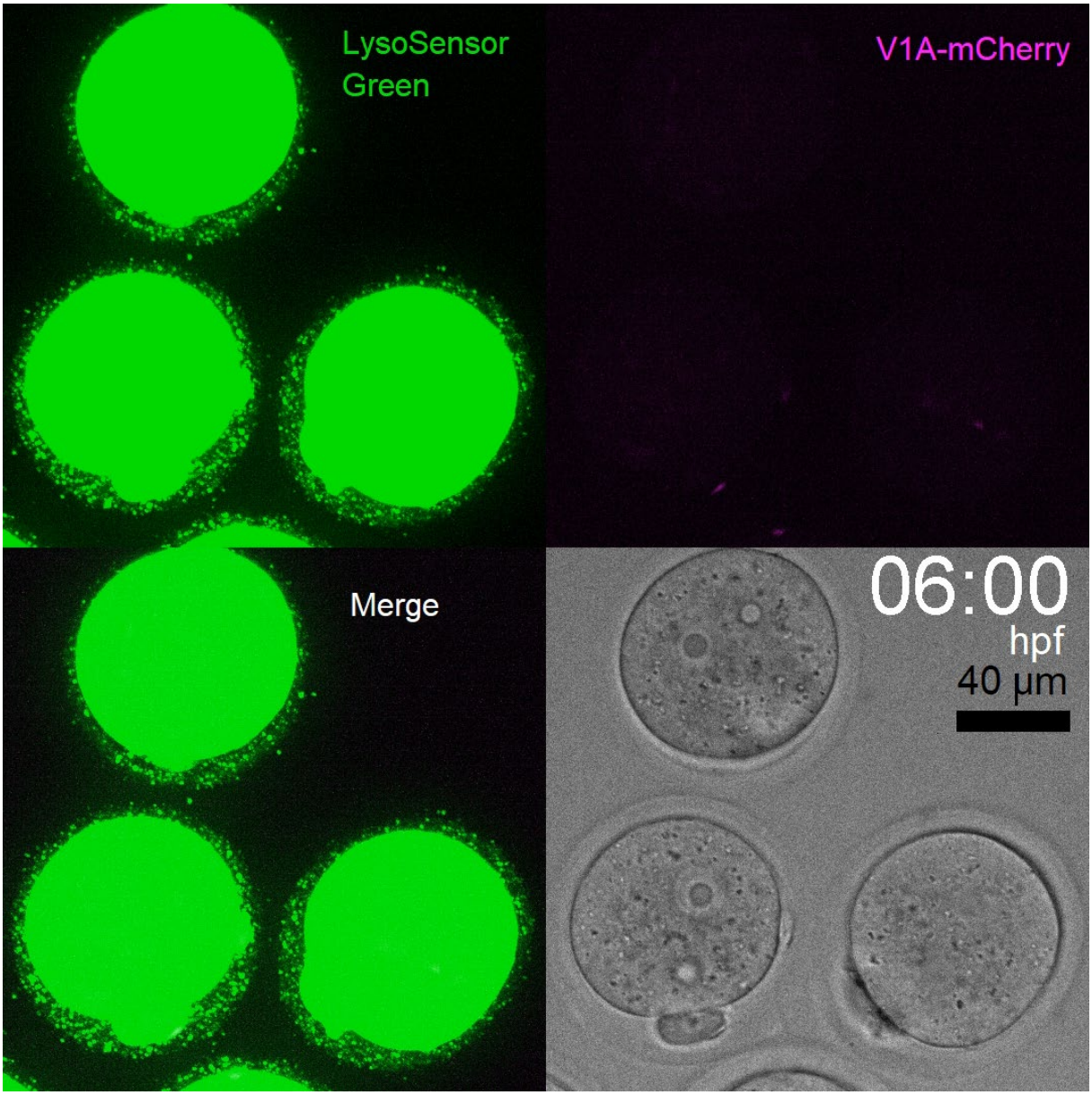

Supplementary Movie 4.
Time-lapse movie of fertilized oocytes expressing V1A-mCherry mRNA in the presence of LysoSensor Green during embryonic development. The maximum intensity projection of confocal images of 80-µm in height is shown.